The Clumping Factor of Intergalatic Gas

Wednesday, 24 May 2023

)
Samuel Gabe (Student ID:)

Abstract: *The objective of this experiment is to explore the clumpiness of gas in the intergalactic medium, specifically how it varies with the dark matter model being examined and if the clumping factor is a signifigant factor in the fraction of ionised hydrogen in the IGM (the ionization fraction) particularly when compared to the ionization emissivity, as well as how the timing and duration of reionization is affected by dark matter models and if dark matter models can be distinguished by their effects on the progression of reionization. This was done via use of the Sherwood-Relics project's suite of hydrodynamical cosmological simulations of the IGM during and immediately after the cosmic reionization of hydrogen. By considering parameters of the IGM as provided by these simulations, it is possible to calculate and compare the clumping factors, ionization fractions, and the timing and duration of reionization for various models of dark matter. This was investigated to question the choice often made in similar cosmological research to treat the clumping factor as a constant value rather than using a more rigorous model under the presumption that other factors dominate. It was found that the clumping factor does differ significantly between different models of dark matter and affects reionization, but that emissivity is overwhelmingly more influential to the timing and duration of reionization. This validates the approaches currently used in most of the field, which ignores the varying of the clumping factor to make simulations more efficient in exchange for losing what has turned out to be a relatively inconsequential detail – with the arguable exception of any study of warm dark matter between redshift 5 and 7, where it is somewhat less inconsequential. It was also shown that the timing and duration of reionization is impacted massively by the dark matter model being used, especially if the mass of the particle being simulated changes, and that observation of the ionization fraction could be used to differentiate between dark matter models.*

1   Introduction

The epoch of reionization is a period in the early Universe approximately 0.2 Gyrs after the Big Bang [1] (between z = 6 and z = 17±4 [2]), which took place after the recombination period. After the Big Bang, the Universe was too hot for neutral atoms (i.e., with orbiting electrons) to exist, so the Universe was made up of ions and electrons. As the Universe expanded it began to cool, and electrons combined with atoms in what is known as the recombination period, which despite its misleading name is the first time atoms existed in this state. Gravitational forces caused gas to coalesce together in halos, making an uneven distribution of mass. These gravitational forces caused the halos to collapse in on themselves, causing an increase in density and hence an increase in temperature. As a result, atoms once again became ionized, hence the reionization epoch started. In this period, the first stars and galaxies began to form in the high redshift universe, each releasing UV radiation to ionize the nearby neutral hydrogen of the IGM into HII. These ionized areas grew and overlapped as the reionization and heating continued until the vast majority of the IGM was inhomogeneously ionized around 0.9 Gyrs after the big bang [1], resulting in an uneven, clumpy IGM which, under the effects of gravity and gas density [3], go on to fuel the formation of stars and galaxies. This is what we refer to as the reionization epoch, which is the beginning of the universe as we know it. Understanding this period is fundamental to understanding the formation of our universe, the current universe in which we live and, most importantly for this investigation, the dark matter model most likely to govern it.

To investigate reionization, we used data from the Sherwood-Relics simulations – a recently developed suite of "hybrid radiation-hydrodynamical models of the Lyman-alpha Forest" [4]. For the purposes of this paper, that means that it is a set of hydrodynamical simulations being used to simulate the intergalactic medium (IGM) during the early universe, and it does this by considering the Lyman-alpha (Lyα) absorption lines generated by light from luminous quasars passing through the IGM. These absorption lines are incredibly useful because the thermal state of the Lyman-alpha forest can retain memory of its heating during reionization, and thus can provide information about redshifts and on scales otherwise inaccessible via any other observable factor [1], and has been shown to be a reliable probe of dark matter distribution [5]. Over the years there have been many attempts at simulating the early universe, from analytical models to N-body simulations to the radiation hydrodynamical simulation suite that we are utilising, in a wide range of effectivenesses and costs. While they are effective, these more complicated simulations are limited by runtime and computational requirements, but this can be alleviated somewhat with hybrid models and post-processing. In this investigation we will employ analytical calculations, numeric data handling, and the results of the Sherwood-Relics project simulations to investigate the effect of dark matter models and the clumping factor on the IGM and reionization.

The Sherwood-Relic Project's predecessor, the Sherwood simulations, had been shown to be largely in agreement with observational data with the minor flaw of assuming a homogenous UV background ionizing the IGM. The Sherwood-Relics Project addresses this by adding a self-consistent model for cosmological radiative transfer [6]. It has also added a great deal of variables to be adjusted which were not accounted for before, allowing the parameters of the Lyα forest to be changed, the use of a range of redshift values, dark matter free streaming scales, dark matter and gas resolutions, dark matter models, and photoheating histories. This puts these simulations far beyond the average suite being used to examine this area and should allow significantly more precise and detailed modelling [5].

The Sherwood-Relic simulations are also an improvement over prior methods in that they do not use post-processing, which is extremely common in earlier work [7, 8, 9] as a way to make up for lacking computing capabilities. Post-processing is useful as it makes programs faster but does not allow for self-consistent models and so sacrifices detail. Instead, the Sherwood-Relic simulations use a hybrid radiation-hydrodynamics model. This means these simulations can account for changes in gas distribution and thermal energy in the gas flows, which is often overlooked [6].

Research in this area is advancing as quickly as technology allows, as the computational cost of the more advanced simulations often acts as a limiting factor. Generally, people have become relatively adept at creating models of CDM, but simulations of WDM are somewhat more novel and the conclusions less certain, being that the model gained popularity as an alternative to CDM relatively recently [10].

The most popular dark matter model currently is Lambda Cold Dark Matter (ΛCDM), a type of CDM that correctly models large scale structure and aligns with the most up-to-date information we have on Cosmic Microwave Background (CMB) temperature and polarization [11]. In that regard it is the most precise to observation model that we have at the moment. However, this still doesn't account for the "small-scale crisis" that plagues ΛCDM, wherein those predictions far overestimate the mass and population of galaxies in areas of length and mass scale below ~ 1 Mpc and $\sim 10^{11} M_\odot$ [12], in addition to other relatively minor issues that, thus far, cannot be resolved by this model. Several warm dark matter candidates, due to having non-negligible free-streaming scales, could resolve the small-scale crisis by suppressing small scale structure and thus fixing the overestimates at low scales - in fact WDM models can act as ΛCDM models, with an extremely similar power spectrum until a cut-off at that lower mass bound, if simulated correctly. Domingo et al. [11], among

others, have demonstrated that, although not currently favoured by the field at large, WDM candidates are still a viable option and that the search for DM candidates is far from settled.

The aim of this investigation was to answer three basic questions. The first was to investigate the effect of dark matter models on the progress and timing of reionization and to determine how signifigant that effect is. Secondly, we aimed to determine if it is possible to distinguish dark matter models through observation of their ionization histories. Thirdly, the effect of the clumping factor and that of the ionising emissivity were investigated and compared to discern which dominates the progress of reionization. Beyond that, we are also seeking to confirm that the current understanding of this era of cosmology is valid, and to validate a mainstream approach for modelling dark matter; if the hitherto widely neglected varying clumping factor *is* significant, then the current convention and literature is based on incomplete models [13, 16]. In part, this investigation is not just to understand the behaviour of the actual universe, but also to test the simulations in use and our understanding of them.

2   Theory

2.1 Dark Matter Models

This project concerns different dark matter models and the variations in how they affect the reionization epoch. Dark matter is a type of matter about which little is known, but which we know to exist due to various physical effects in the Universe, such as gravitational lensing of galaxies. It is thought to be comprised of heavy particles and makes up about 25% of the mass of the Universe (Klasen et al., 2015) [14]. The most widely accepted dark matter model assumed to be the most accurate in describing dark matter in our universe is the Lambda Cold Dark Matter model (ΛCDM). The ΛCDM used here is the fiducial ΛCDM model developed by Puchwein et al. [15]. The "Λ" refers to the fact that this model takes account of dark matter, and its inclusion in the name is largely a matter of convention as this is now often taken as the standard model of dark matter. It is generally considered appropriate to refer to it as simply CDM [15], and we will do the same here. The Sherwood-Relics simulations used to generate the data in this project contain data obtained from using seven dark matter models, which are grouped into three ΛCDM models and four WDM models.

The three CDM models used here are identical to one another aside from their photoheating rates, which is doubled in the case of the hotter model and halved in the case of the colder one [3], which adjusts their average gas temperature without altering any other property. This is allowable both because the actual temperature of the IGM at early redshifts is not a concretely known quantity, and because this is an exercise in curiosity; if the IGM had a higher or lower temperature, what effect would that have, and would it align with our current understanding of the ionization progress of the era? The main variation in the warm dark matter models is the mass of the dark matter particles. In our results, the four warm dark matter models are referred to as 'WDM1', 'WDM 2', 'WDM3' and 'WDM4', where the number suffixing WDM refers to the mass of dark matter particles in keV/c^2 (WDM1 has a mass of 1 keV/c^2, WDM2 has a mass of 2 keV/c^2, and so on). The properties being modelled in these seven versions of dark matter are not any specific "real" dark matter candidates, but rather generalised properties which *approximate* several classes of candidate in consideration (e.g., WIMPS, axions, and sterile neutrinos) – a much more intricately detailed discussion of these models can be found in Puchwein et al., 2020 [15].

Warm dark matter models have the slightly odd trait of supressing small-scale structure, meaning that they cause a larger amount of the mass present in the universe to congregate close together and so leaving comparatively little mass to build small structures in the IGM. This occurs more markedly in models with lower mass particles. This is because a DM model with lower mass has a higher free streaming scale, which quantifies the distance over which the particle can move without being scattered or absorbed and is directly related to velocity (and thereby mass) [18]. This originates in the density field perturbations with which the simulation is initialised, which are determined based on matter power spectrums inferred from the cosmic microwave background [19]. Due to gravity and the nature of hierarchical structure formation, these perturbations grow over time, more so (in comparison to the rest of the simulation volume) if particle's free streaming scale is higher. The reason this erasure is only mentioned in reference to WDM is that CDM models tend to have *much* heavier particles – while the WDM models have masses in the order of keV/c^2, the CDM models are of the order of GeV/c^2 and as such their free-streaming scales are negligible. The presence of small-scall structure suppression in WDM is one of the reasons it is being considered as serious contender against ΛCDM; it could hold the key to solving the small-scale crisis [12].

In these experiments, each of the seven dark matter models mentioned were investigated along with the differences in how each one affects the progress of reionization. There are two factors which vary based on the dark matter model being used: the clumping factor, and the ionizing emissivity, both of which are discussed in the following sections.

2.2 Ionization Equation

The ionization equation is a first order differential equation which can be solved to find the ionization fraction. This equation was proposed in Madau et al., 1999 [20], but numerous enhancements to this model have been presented over the years (see Kaurov & Gnedin 2015; Jeeson-Daniel et al., 2014 [21, 22]).

The ionization equation is given as [23]

$$\frac{dQ}{dz} = \frac{1}{H(z)(1+z)}\left(\frac{Q}{\bar{t}_{rec}} - \frac{\dot{n}_{ion}}{\bar{n}_H}\right),\tag{1}$$

where z is the redshift, $H(z)$ is the Hubble parameter, $\bar{t}_{rec}$ is the recombination timescale (as defined in Equation 2), $\dot{n}_{ion}$ is the reionizing emissivity which will be discussed in Section 2.4 and $\bar{n}_H$ is the mean density of hydrogen in the Universe.

The Hubble parameter, $H(z) = H_0\sqrt{\Omega_M(1+z)^3 + \Omega_\Lambda + \Omega_K(1+z)^2}$, where H_0 is the Hubble constant and the Ω terms refer to the ratio of density to the critical density ρ_c of the Universe – for example, $\Omega_M = \frac{\rho_M}{\rho_c}$. Here Ω_M refers to matter in the Universe including dark matter, Ω_Λ is associated with the cosmological constant Λ and is closely related to dark energy, and Ω_K is the contribution from the shape of the Universe. The critical density of the Universe ρ_c is the density at which the expansion of the Universe is neither accelerating or decelerating. Currently, the density of the Universe is thought to be roughly equal to ρ_c, corresponding to a flat Universe. Ω_K is either positive, negative or zero depending on the 'shape' of the Universe, and for a flat Universe it is equal to zero, so this term can be neglected in the Hubble parameter.

The recombination timescale $\bar{t}_{rec}$ is the volume average gas recombination time given by

$$\bar{t}_{rec} = C\alpha(T)\bar{n}_H(1 + z)^3 \left(1 + \frac{Y}{4X}\right)^{-1}. \tag{2}$$

The C term here is the way in which the clumping factor impacts reionization [7].

2.3 The Clumping Factor

The 'clumping factor' is the quantity which accounts for the effect of recombination in unresolved small-scale structure in the IGM on ionization calculations and describes how uneven the distribution of matter is in the Universe. During the recombination period, matter was very evenly spread and the Universe was homogeneous. However, gravitational forces caused matter to 'clump' together into halos. The clumping factor is essentially a way of quantifying this 'clumpiness'. A higher clumping factor corresponds to higher discrepancy between the highest density regions and lowest density regions of the Universe.

The clumping factor varies locally, relies on the halo mass function, and has been demonstrated by Kaurov and Gnedin [24] to add significant corrections to their recombination rate when compared to uniform clumping, as would be expected given the factor's heavy involvement in Equations 2 and 3. Despite this, cutting edge modern simulations can often relegate the clumping factor to subgrid modules due to computational difficulty in finding the clumping factor of the gas directly because of a lack of resolution. It's also not unheard of for simulations to entirely ignore hydrodynamics and assume that gas will follow the dark matter [25]. For instance, the SCORCH. III model by Chen et al. [7] is from only two years ago and uses the clumping factor in its subgrid modelling to compensate for fluctuations in recombination and photoionization rather than a self-consistent local model. This functions, but, for such a vital factor, seems questionable and can be improved. Addressing this issue by properly investigating the clumping factor as a crucial factor which is worth examining in detail due to its impact on the timing and duration of reionization is a signifigant part of the goal of this project.

One of the simplest definitions of the clumping factor was presented in Madau et al., 1999 [20]. It is given by one of two very similar equations:

$$C_G = \frac{\langle \rho^2 \rangle}{\langle \rho \rangle^2}, \tag{3}$$

$$C_N = \frac{\langle n^2 \rangle}{\langle n \rangle^2}, \tag{4}$$

where ρ is the gas density and n is the gas number density. These two equations have a fundamental flaw in they take account of all material in the volume, making no distinction as to whether that material is relevant to recombination. There are many definitions of the clumping factor which have been used over the years [25] and some are considered to be more reliable. As this project concerns the ionization fraction of the universe, it is better to use a clumping factor which specifically concerns the ionized hydrogen in the universe. We can write this as

$$C_{HII} = \frac{\langle n_e n_{HII} \rangle}{\langle n_e \rangle \langle n_{HII} \rangle}, \tag{5}$$

where n_{HII} is the number density of ionized hydrogen nuclei and n_e is the number density of electrons. We can further elaborate on this model by factoring in the recombination coefficient

$\alpha(T)$, which is a measure of the rate of recombination of atoms. Factoring in this recombination coefficient gives a further improved definition of the clumping factor, called the recombination clumping factor, or C_R, expressed as [20]

$$C_R = \frac{\langle \alpha(T) n_e n_{HII} \rangle}{\langle \alpha(T) \rangle \langle n_e \rangle \langle n_{HII} \rangle}. \tag{6}$$

2.3.1 Terms in the clumping factor

In order to calculate the clumping factor, we need to find values for n_e, n_{HII} and $\alpha(T)$. The number density of ionized hydrogen, n_{HII}, can be expressed as

$$n_{HII} = n_H(1 - X_H), \tag{7}$$

where n_H is the total hydrogen gas number density and X_H is the fraction of gas which is hydrogen. We can use this to give a definition of the electron number density [20],

$$n_e = \left(1 + \frac{Y_{He}}{4X_H}\right) n_{HII}, \tag{8}$$

where Y_{He} is the helium fraction of the gas. Finally, the recombination coefficient is written as [26]

$$\alpha(T) = 4.06 \times 10^{-19} \mathrm{m}^3 \mathrm{s}^{-1} \left(\frac{T}{10^4 \mathrm{K}}\right)^{-0.72}, \tag{9}$$

where we have used a constant scaling term from observational data. The values of n_H, X_H, Y_{He} and T can be found in the simulation data, so we now have a usable model for clumping factor.

2.3.2 Derivation of the Clumping Factor

In order to find the clumping factor, we start with the ionization equation in a different form, given by [7]

$$\frac{dn_{HII}}{dt} = \Gamma_{\mathrm{HI}} n_{HI} - n_e n_{HII} \alpha(T), \tag{10}$$

where Γ_{HI} is the photoionization rate and $\alpha(T)$ is the recombination coefficient. This is the ionization equation taking into account the photoionization rate as opposed to the ionizing emissivity. When averaging over some volume V, this becomes

$$\frac{d}{dt} \langle n_{HII} \rangle_V = \Gamma_{\mathrm{HI}} \langle n_{HI} \rangle_V - \langle n_e n_{HII} \alpha(T) \rangle_V. \tag{11}$$

The second term on the right-hand side can be modified to introduce the clumping factor into the equation,

$$\frac{d}{dt} \langle n_{HII} \rangle_V = \Gamma_{\mathrm{HI}} \langle n_{HI} \rangle_V - \langle n_e \rangle_V \langle n_{HII} \rangle_V \langle \alpha(T) \rangle_V \frac{\langle n_e n_{HII} \alpha(T) \rangle_V}{\langle n_e \rangle_V \langle n_{HII} \rangle_V \langle \alpha(T) \rangle_V}, \tag{12}$$

Now it is trivial to modify the final term to include the clumping factor,

$$\frac{d}{dt} \langle n_{HII} \rangle_V = \Gamma_{\mathrm{HI}} \langle n_{HI} \rangle_V - \langle n_e \rangle_V \langle n_{HII} \rangle_V \langle \alpha(T) \rangle_V C_R. \tag{13}$$

2.4 Ionizing Emissivity

As well as the clumping factor, the ionizing emissivity term $\dot{n}_{ion}$ plays a role in the progression of reionization. $\dot{n}_{ion}$ is defined as the number of ionizing photons emitted per unit volume per unit time. These ionizing photons are emitted when ionized photons recombine – despite the ionization fraction increasing in the reionization period, newly ionized atoms will still recombine, and this will slow the rate at which the ionization fraction increases. We can model this to varying degrees of complexity. The model used in this project is written as [27]

$$\dot{n}_{ion} = \zeta \frac{\sum_i (M^{i^{(\alpha)}})}{V_{box}}, \tag{14}$$

where ζ is a constant which we can adjust to fit to the observed data, $\sum_i (M^i)$ is the sum of the halo masses and V_{box} is the volume of the area (or simulation "box") which we are observing. $\dot{n}_{ion}$ is effectively proportional to the density of the IGM. The exponent α is an optional adjustment to allow $\dot{n}_{ion}$ to vary nonlinearly with halo mass. Finlator et al., 2011 [28] found that for halo masses ranging from $10^{8.2}$ to $10^{10.2}$ M$_\odot$, α is in the range of 1.3-1.4. However, largely, for this project a linear relation between halo mass and ionizing emissivity has been assumed. This is a simplified model which could be greatly improved by the introduction of more, and more carefully adjusted, parameters with which to calibrate $\dot{n}_{ion}$ against realistic measurements.

3 Investigating the clumping factor

3.1 The different definitions of C

This investigation was carried out entirely computationally using data detailing the epoch of reionization as simulated by the Sherwood-Relic hybrid hydrodynamical Lyman-alpha suites, which was read from local binary files supplied by the University of Nottingham and the Sherwood Relic program [17]. The size of these files caused some storage problems, which were circumvented via use of cloud storage and converting particularly relevant information into different file types.

Due to the theoretical nature of this investigation and the use of simulation data rather than any measured quantities, there are no numeric uncertainties on any results found, but the trends explored should be of use when compared to other research and expectations.
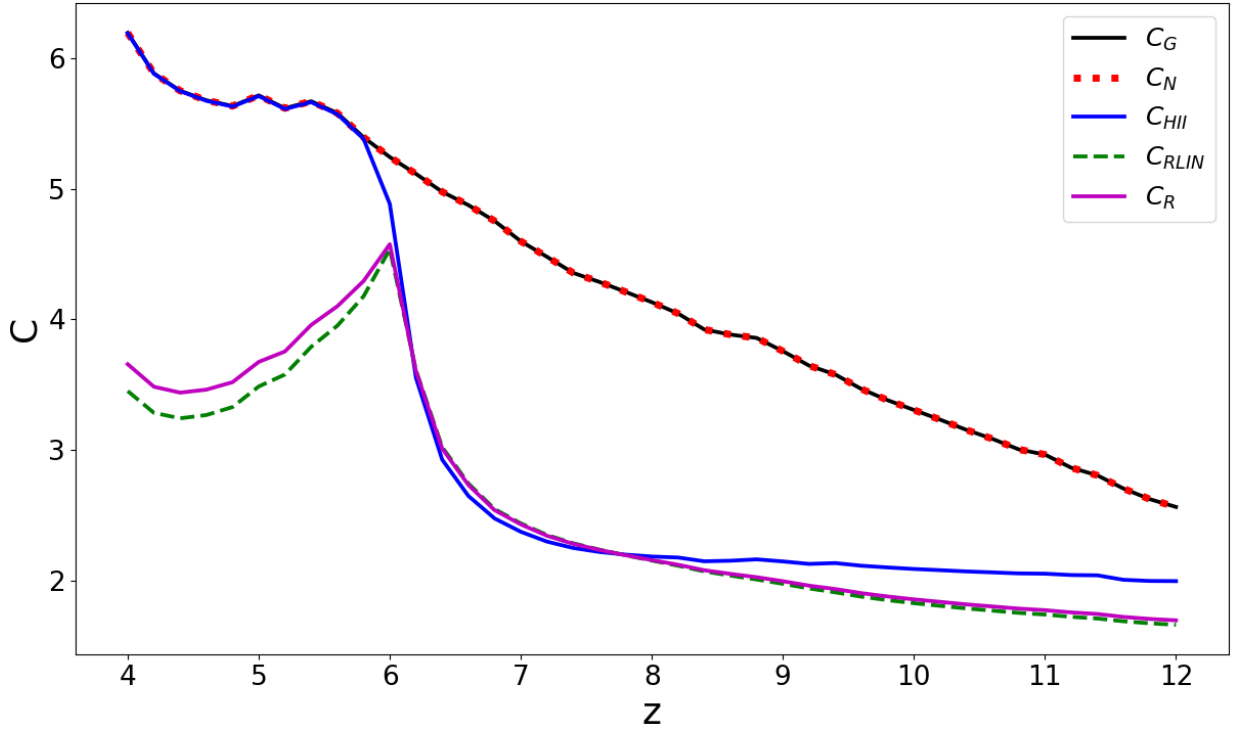
Figure 1 – A plot comparing all five of the clumping factor definitions examined in this paper, as detailed in Section 2.3. These values of C were calculated for the default ΛCDM model, but a very similar set of curves was seen in all models.

The definitions of the clumping factor as laid out in Section 2.3 (Equations 3-6) were investigated over the range of redshifts appropriate for this simulation (redshift 12 to 4) and which should include all information relevant to reionization for our purposes [23]. Each definition of C was calculated and plotted against one another in Figure 1 to visualise their differences and help determine which to use. Each definition of C is dimensionless due to being based on density ratios.

C_{RLIN} and C_R are both calculated as in Equation 6, with the difference being that C_{RLIN} approximates the recombination coefficient $\alpha(T)$ as shown in equation 9, whereas C_R calculates it according to a very detailed fit developed by Verner and Ferland (1996) [26]. Both definitions were evaluated - the differences between the two types of C_R are shown in Figure 1 and the differences in $\alpha(T)$ which caused them in Figure 2.
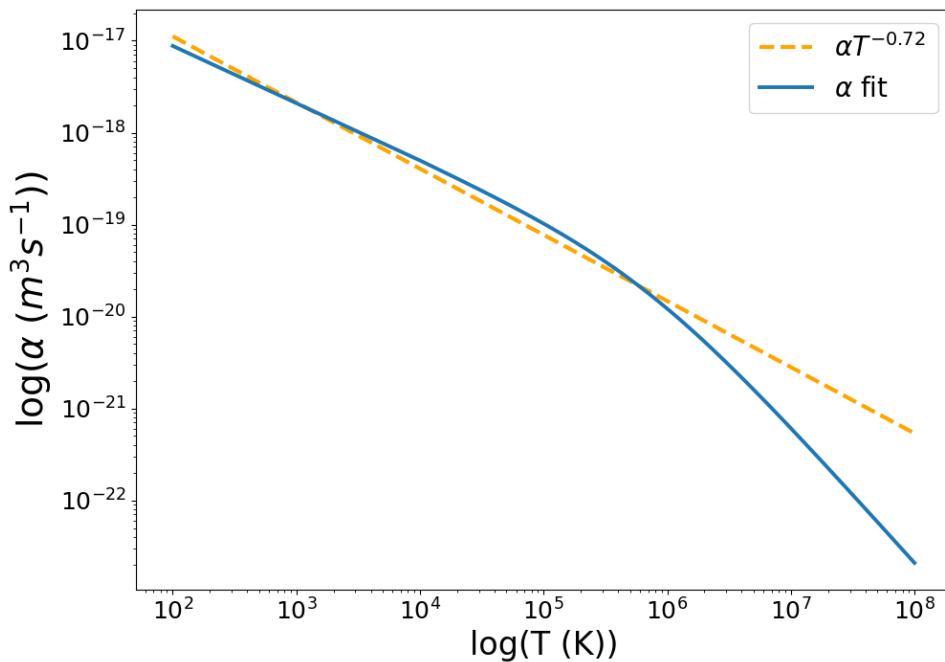
Figure 2 – A plot of the two possible versions of the recombination coefficient, one as the linear relationship used in C_{RLIN} and one as the fit used in C_R. This was found using the default ΛCDM model.

It was ultimately found that the difference that the Verner and Ferland fit caused in the values of C_R were significant, and so that is the version of C_R used throughout.

The factors which comprise the clumping factor were also investigated as a means to verify that the data being obtained aligns with our understanding of this period and that C varies with them as expected. This is shown in Figure 3, along with a comparison of the three definitions of C found to be relevant (i.e., not degenerate or incorrectly fitted).
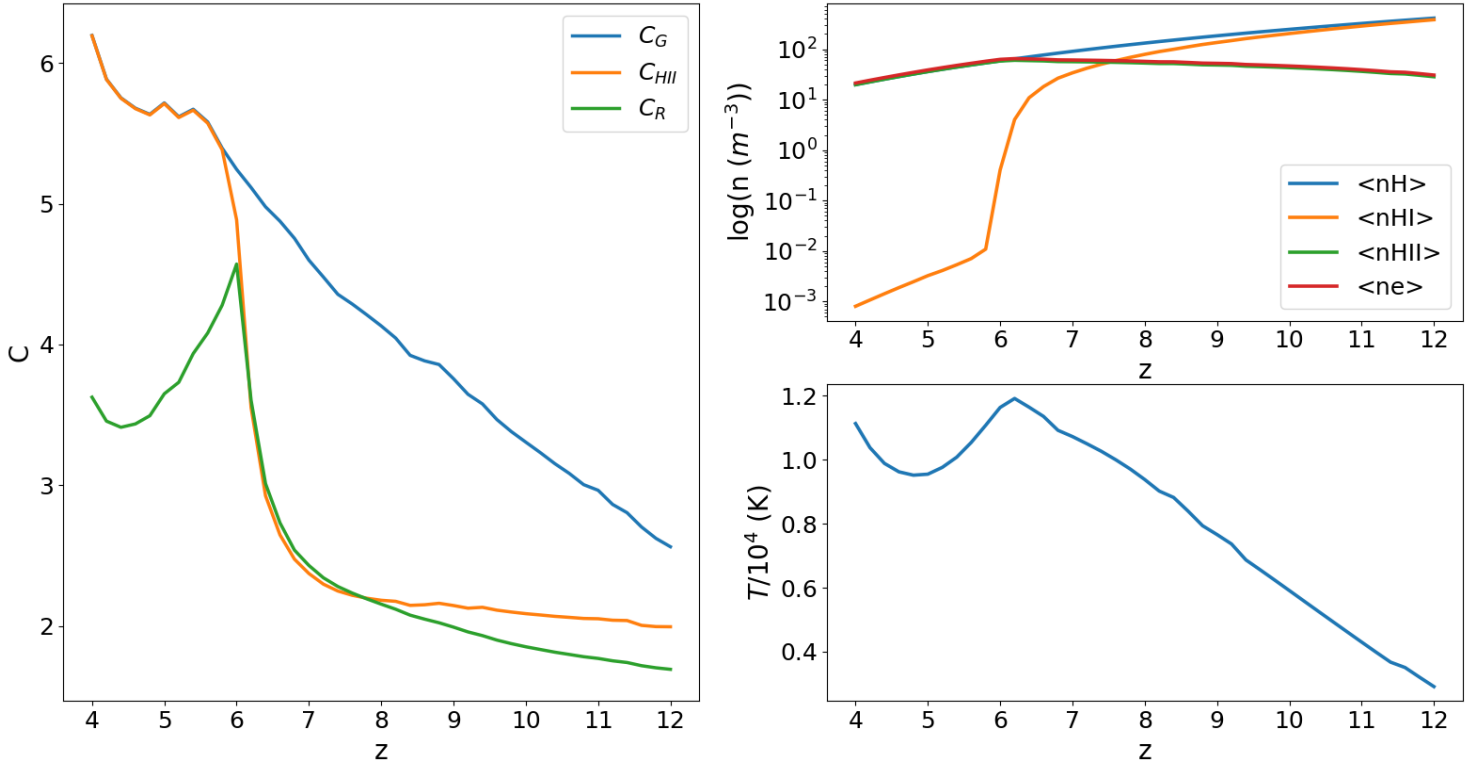
Figure 3 – a set of subplots showing the three definitions of C which will be investigated here, the average number densities of the components of C, and the average temperature of the simulation volume, all of which are plotted against redshift. These values were calculated for the default ΛCDM model.

Another definition was investigated in addition to these mentioned, the number density definition, C_N, which calculates C in accordance with relative number densities as in Equation 4, but this was found to be effectively identical to C_G at every point and on every scale, and so has been omitted.

3.2 Density Limits

The calculation of the clumping factor requires a density limit to impose a cut-off point to determine which areas of the simulation are considered to be in the IGM and which instead represent part of the populated universe. Here, this takes that form of the ratio between the density of the volume being examined and the density of the box overall. Areas above the density limit are not taken into consideration because they are too densely populated and impenetrable to allow any signifigant

amount of the hydrogen there to be ionized [7]. The three definitions of C ultimately being examined were evaluated at multiple density limits to examine its effects, as shown in Figure 4.
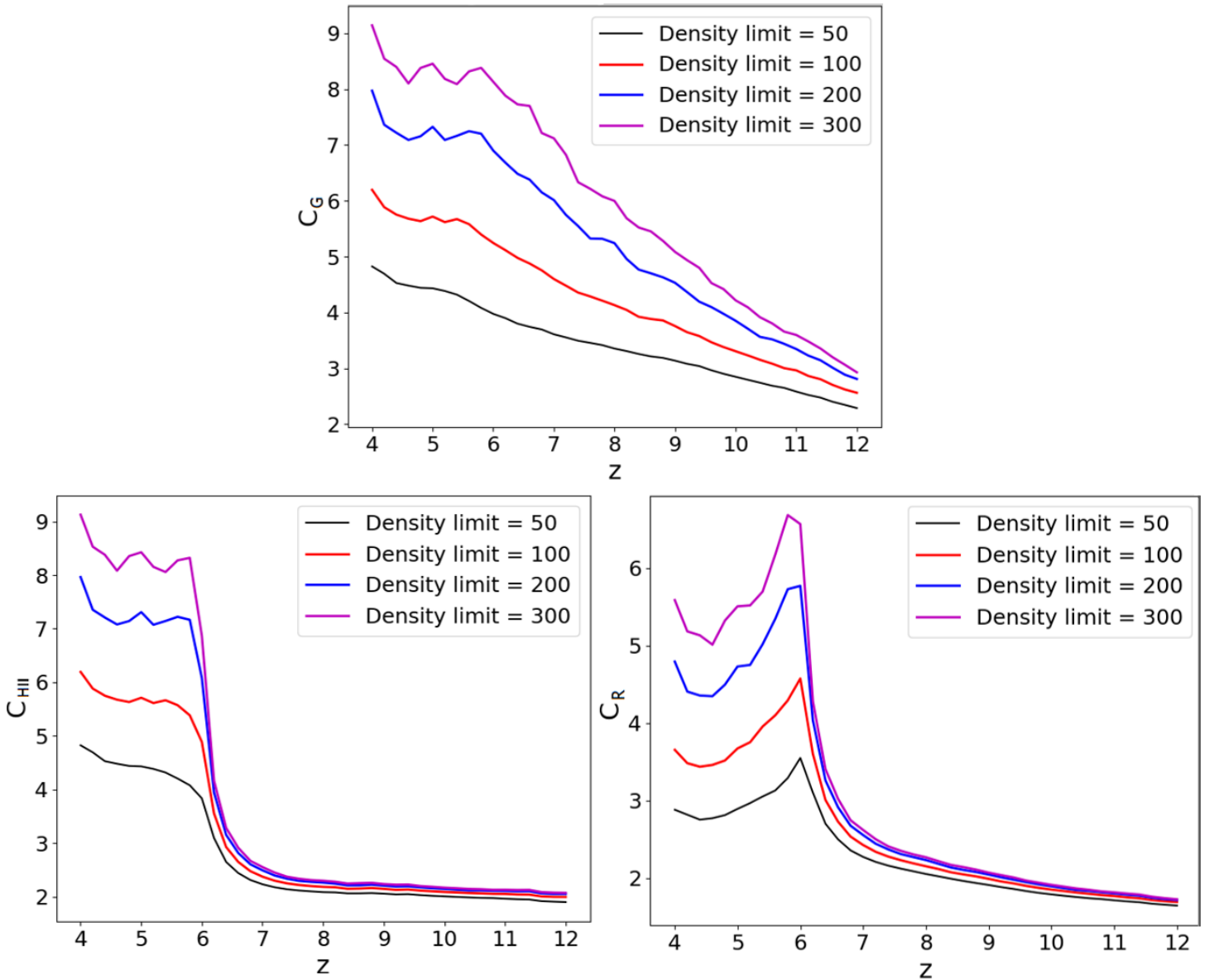

Figure 4 – The three relevant definitions of C evaluated at different density limits. This was performed using the default ΛCDM model.

3.3 The clumping factors of all models

The three relevant definitions of C were calculated for each dark matter models being investigated and are shown in Figure 5. Problems were encountered in terms of computing time, even after the code had repeatedly been optimised for speed, so the values of C were calculated individually for each model from the Sherwood-Relic data and then saved in plain text files so as to allow them to be accessed easier and to save on time and computational requirements, which are very typical limiting factors in the field [5]. The original data was deleted at this point, computationally burdensome and rendered unnecessary.
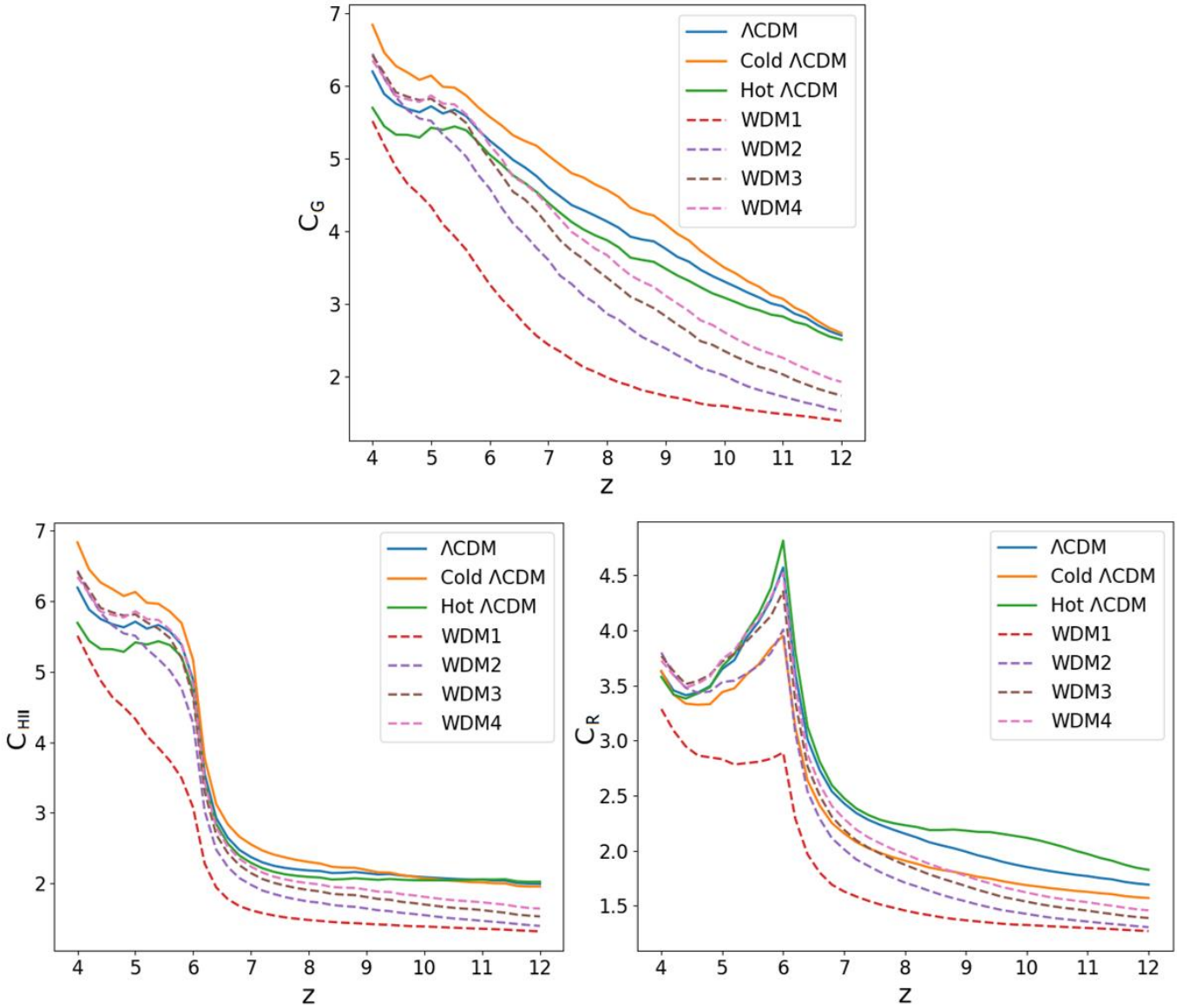
Figure 5 – The three relevant definitions of C evaluated at a density limit of 100 for all 7 models of dark matter being examined.

3.4 Discussion

The clumping factor can be a somewhat nonspecific term in that it has many mathematical definitions, all of which produce different ranges of values. It was found in Section 3.1 that the C_{HII} definition is more accurate than C_G, in that it only takes account of the number density of electrons and ionized hydrogen, the only particles which are relevant when it comes to hydrogen recombination, while the recombination clumping factor, C_R, improves upon that by including a temperature dependence via use of the recombination coefficient $\alpha(T)$, which has an approximate trend of $\alpha \propto T^{-0.72}$ (as in equation 9), but it was shown in Figure 1 that differences caused by the more detailed fit given by Verner and Ferland [26] is significant, especially at high temperatures, which is when the intricacies of the temperature-dependant C_R are of particular note. This can be seen in Figure 1, where C_{RLIN} and C_R are practically identical until temperature peaks at z ≈ 6.

The inclusion of this temperature reliance is an improvement because it reflects the effects of temperature on recombination rates [7], and the fact that the C_{HII} definition models the recombination coefficient $\alpha(T)$ as a constant (with a value of 1) is purely unphysical. C_{RLIN} modelling $\alpha(T)$ as in Equation 9 *is* more viable than C_{HII}'s method, but C_R was determined to be a

more suitable definition. Hence, from Section 4 onwards, it can be assumed that whenever the clumping factor C is mentioned, it refers to the fit recombination clumping factor C_R.

The changes in the number densities of the components of the IGM over time in figure 3 are reassuring, in that they show the exact trends which were expected [11]: the amount of unionized hydrogen plummets as ionized hydrogen rises, full reionization occurs just before redshift 6, the sum of both never exceeds the amount of hydrogen in total, and the number densities of electrons and of ionized hydrogen are very closely tied together almost to the point of being identical, due to the fact that hydrogen ionization would be by far the largest source of electrons in the IGM over that period. These *are* average number densities though, meaning that they will not form a completely accurate and comprehensive picture of the universe, but that can also be said for these simulations in general; what is being examined here is the trends, and those do hold true. This could be improved somewhat by adjusting the way in which these number densities are calculated such that only parts of the simulation box with a density limit ratio of approximately 1 are considered; these represent relatively very stable areas of the IGM and would give more reliable average number densities. Any uncertainty in this section is likely to arise from the use of these unadjusted total average number densities, both here and in all the clumping factor definitions in Equations 3 to 6.

   The temperature trend in Figure 3 is also as expected, with the average temperature of the IGM rising steadily until all hydrogen present is fully ionization, dipping, and then beginning to rise again after redshift 5, showing that helium ionization has begun. Altogether this indicates both that the data being pulled from the simulation is valid and that it is being read and processed correctly. It can be seen in Figure 3 that there is a quite predictable correlation between $\langle n_{HII} \rangle$, $\langle n_e \rangle$, and C_{HII} and C_R, and a strong correlation between the average temperature of the box and C_R, which is particularly visible just before redshift 6, where we would expect to see the impact of reionization. In fact, all the plots in figure 3 show synchronous unique behaviour at that point. These trends are again expected and reassuring, as they align very well with what would be expected for the mathematical definitions of C being laid out in Section 2.3 and indicate that our understanding of these concepts is accurate and that the data is being processed correctly (which is vitally important because this data is the basis for the entire investigation).

Figure 4 shows that the measurements most accurate to expectations were found at a density limit of 100, which also lines with the literature where 100 has been taken as the general convention [25, 29]. This indicates that both that the data used here is correct and being processed correctly, and that a density limit of 100 is an appropriate number to carry forward throughout this investigation. From here on, it can be assumed that the clumping factor is always being calculated at a density limit of 100.

In each plot in Figure 5, all seven curves follow the same approximate trends, similar to those shown in figure 1 and 4, although it should be noted that, despite following the same trajectory in each case, the WDM curves are consistently slightly lower in magnitude than the CDM curves, and the CDM curves are more severe while the WDM curves are slightly more rounded. This can be accredited to the fact that WDM models suppress small-scale structure, which is also why WDM1 is always the lowest of the WDM models in Figure 5 and WDM4 the highest; less small-scale structure means less structure in general in the IGM which still passes below the density limit, and so less mass is centred in areas which are easily photoionized and considered in our investigation. So the areas being investigated in when using WDM are literally less clumpy (the matter in them is less 'clumped up'), and so the clumping factor is lower. As expected, this occurs more strongly in the models with lighter particles.

The CDM models' curves are different from one another too, even in the C_G and C_{HII} plots of Figure 5, which show definitions of C with no direct reliance on temperature. This is somewhat counterintuitive given that the three CDM models are *only* separated by the overall average gas temperature of the box. This is due to the way that, when modelling something as an ideal gas and keeping all other factors constant, temperature and pressure are directly proportional – a higher temperature over the simulation volume leads to a higher pressure and thus a smoother, more homogenous IGM which is less clumpy. For this reason, the cold ΛCDM model consistently has the highest clumping factor, followed by ΛCDM, then hot ΛCDM. The C_R plot is an exception to this, where the temperature dependence of the recombination coefficient overwhelms this effect. Altogether, this shows that the theory outlined in Section 2.1 is sound and gives a very clear sign that the clumping factor *does* vary with DM model and that, if the clumping factor influences reionization with any significance, dark matter models *will* impact ionization histories.

4   The ionization fraction and its relation to the clumping factor

The ionization fraction, Q, defined in equation 1, is the fraction of hydrogen ions to unionized hydrogen in the IGM. It can be plotted to track the progress of the simulation towards full reionization (this progress is what is referred to as the "reionization history") and is an insightful measure of the evolution of the early universe. Due to being a ratio, it peaks at 1, the point at which all hydrogen in the IGM has been ionized.

4.1 Calculating Q without emissivity reliance

Since some of the most obvious libraries which would typically be used for solving differential equations proved to be inviable due to the extremely wide range of the magnitudes of the values being processed, a way of using Euler's method to solve the ionization equation was coded from the ground up. In order to ensure that this was a reliable way of solving Equation 1, since this method would form the basis of the entire rest of the investigation, it was used to reproduce test cases to verify that it could replicate an extremely simple curve given set data. It was shown to be consistently capable of producing correct derivative curves, and so was carried forwards through this investigation.
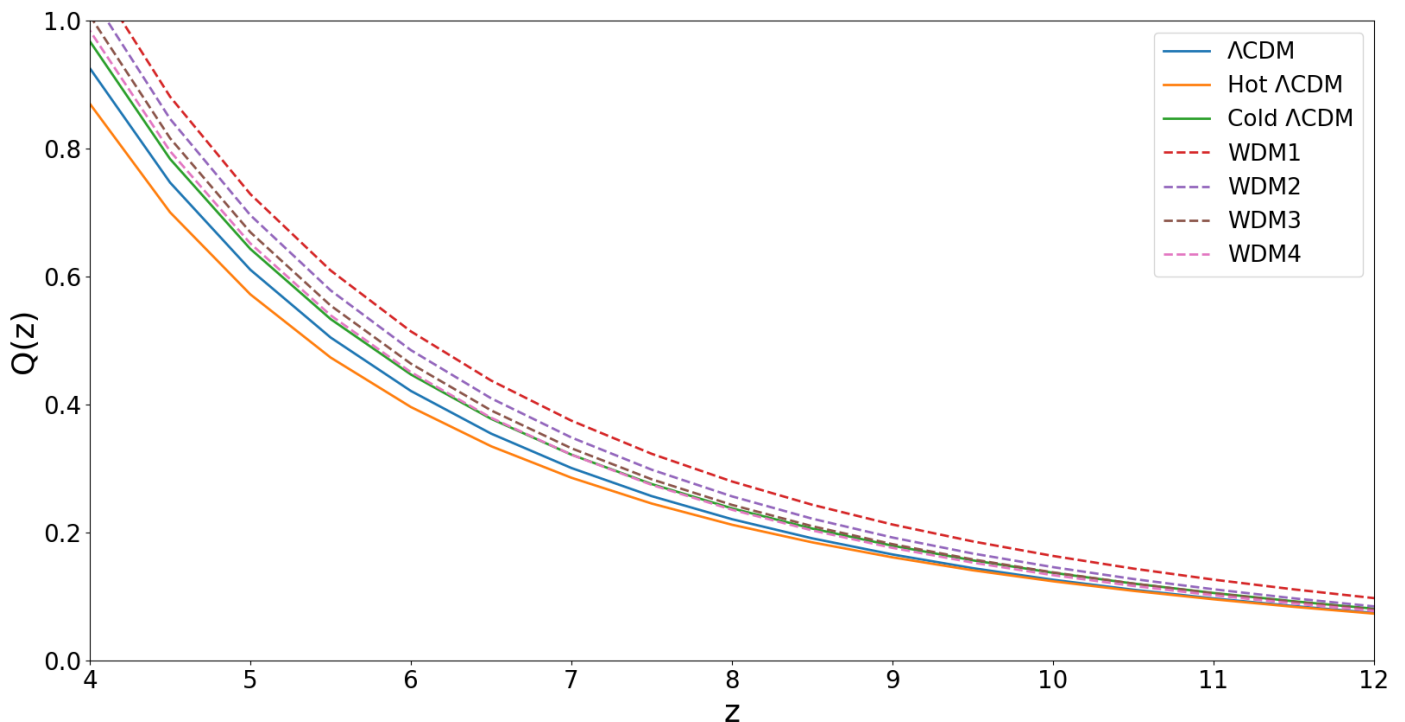

Figure 6 - The ionization fraction for each model of dark matter, as calculated with a constant value of emissivity.

The ionization fraction was first calculated for each model without regard for the way that emissivity varies with redshift (caused by changes in mass which vary with redshift), taking $\dot{n}_{ion}$ as a constant value $\dot{n}_{ion} = 3 \times 10^{50}$ s^{-1} cMpc^{-3} due to the fact that it is a typical value, in line with values from other research [27]. This is shown in Figure 6.

These calculations were then run again using values of $\dot{n}_{ion}$ which *do* vary with redshift, via use of a table of values taken from the simulations found by Kulkarni et al. [27]. The results are shown in Figure 7.
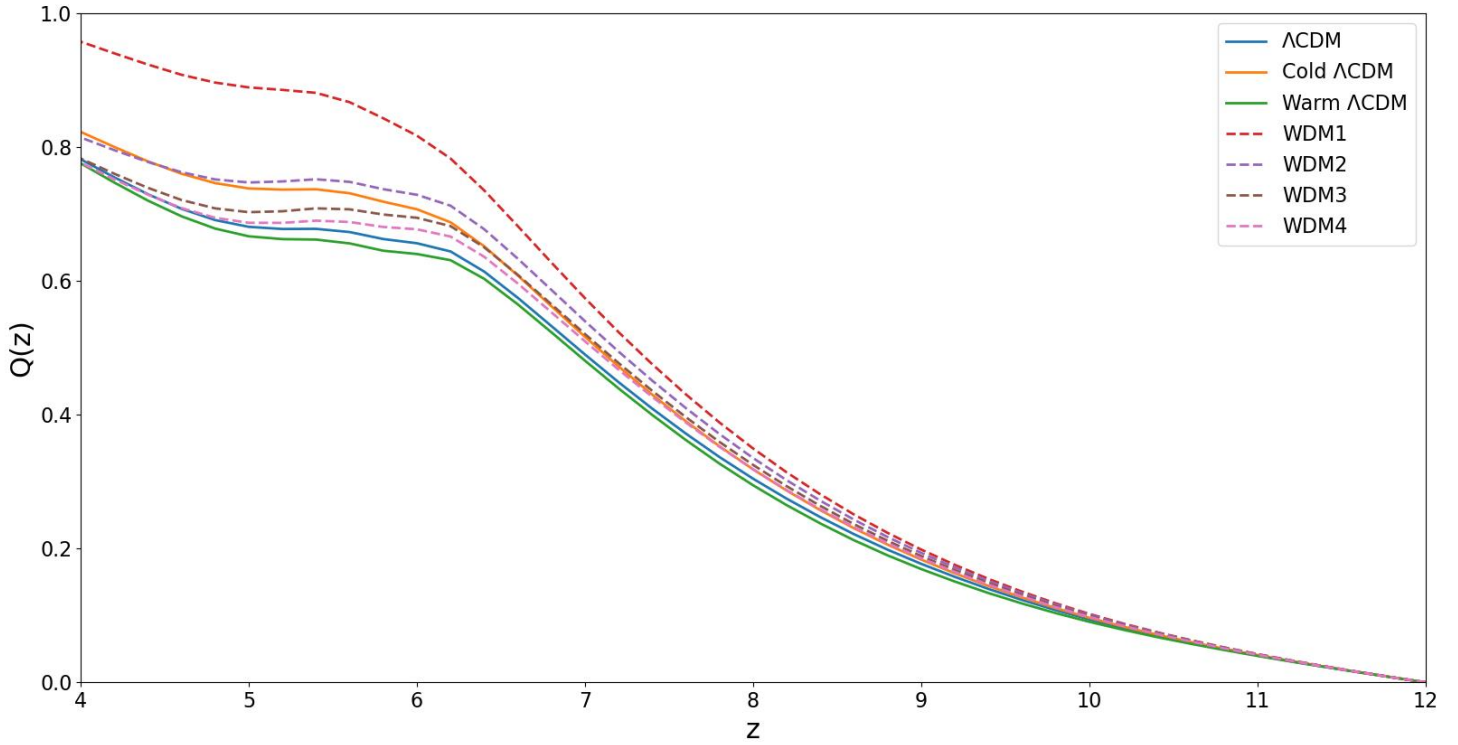

Figure 7 - The ionization fraction for each model of dark matter, as calculated with a set of stand-in values of emissivity that vary with redshift. This is a valid enough approximation of the patterns we should be seeing and demonstrates that nion has a signifigant influence on Q.

It is worth noting, though, that these emissivities, while much more reminiscent of accurate values, are taken from a different simulation which will inherently have different properties than the simulation and models used here, and thus will also have different values of emissivity. These emissivity values were simply used to approximate the way in which Q should change with redshift and to determine if that is a significant relationship, i.e., if it is worth investigating more seriously using data pulled from the Sherwood-Relic simulations which would be accurate to the set-up used here.

4.2 Discussion

The reionization curves shown in Figure 6 are calculated with absolutely no regard to emissivity, which is taken as a constant, with the only variables being considered being redshift, component number densities, and the clumping factor, as in Equations 1 and 2. Although all those quantities do change with the DM model, they change consistently and will do so in every possible variation of our Q plots, so they are largely irrelevant to the comparisons being made in this paper and it is safe to disregard them when it comes to analysis. The only relevant quantity changing between the

ionization histories in Figure 6 is the clumping factor, and as such this might be used to get an approximate picture of its effects - the ionization curves are clustered very closely together, suggesting that the changes caused by C alone are minimal.

The values of Q never exceed 1 in Figure 6 and have the expected shape of (part of) an ionization curve [3], which is a good sign that these calculations, as approximated as they may be, are roughly appropriate and that the clumping factors found in Section 2.3 are of the correct magnitude and trends. Although, an ionization curve should hit $Q \approx 1$ and then stay there, representing total reionization, which these curves do not, meaning that a varying emissivity is vital to producing realistic ionization histories. This is addressed in Figure 7, wherein the use of $\dot{n}_{ion}$ values which vary with redshift cause the curves to exhibit much more typical behaviour by levelling out just before redshift 6, however this is still improper as the Q values level out at $Q \approx 0.8$ instead of 1 and begin to rise again after redshift 5, but this does demonstrate the sizable impact which emissivity has on reionization histories, even when not optimised.

Overall, the results found in this section were not as informative as may be liked, but the results found and code developed therein do lay nessecary groundwork for investigating Q more effectively in Section 5.

5   The HII fraction with varying emissivity

5.1 Halo Mass

Emissivity, as shown in Equation 14, directly depends upon the sum of the halo masses (over a set minimum mass limit) within the simulation volume, which varies with redshift. The mass limit is a product of the limitations of the simulation; approximately $2.53 \times 10^7 \ M_{\odot}$ is the resolution of the simulation and it cannot reliably differentiate objects of a lower mass. After some experimentation, in order to ensure that the highest possible amount of data be considered without reducing accuracy by allowing in potential errors caused by stretching the simulation's data beyond its proper limits, the mass limit was set to the resolution.

The halo masses in the simulation for each model were read, processed, and classified by size into 25 bins and then the number of halos per log mass bin plotted, as shown in Figure 8. This was done at multiple values of redshift in order to examine the ways in which warm and cold dark matter models effect the structure of the IGM and how that varies with redshift.

A similar process was conducted with just one dark matter model (ΛCDM, which has been used as a benchmark throughout) in Figure 9 to demonstrate the way in which structure varies with redshift alone.
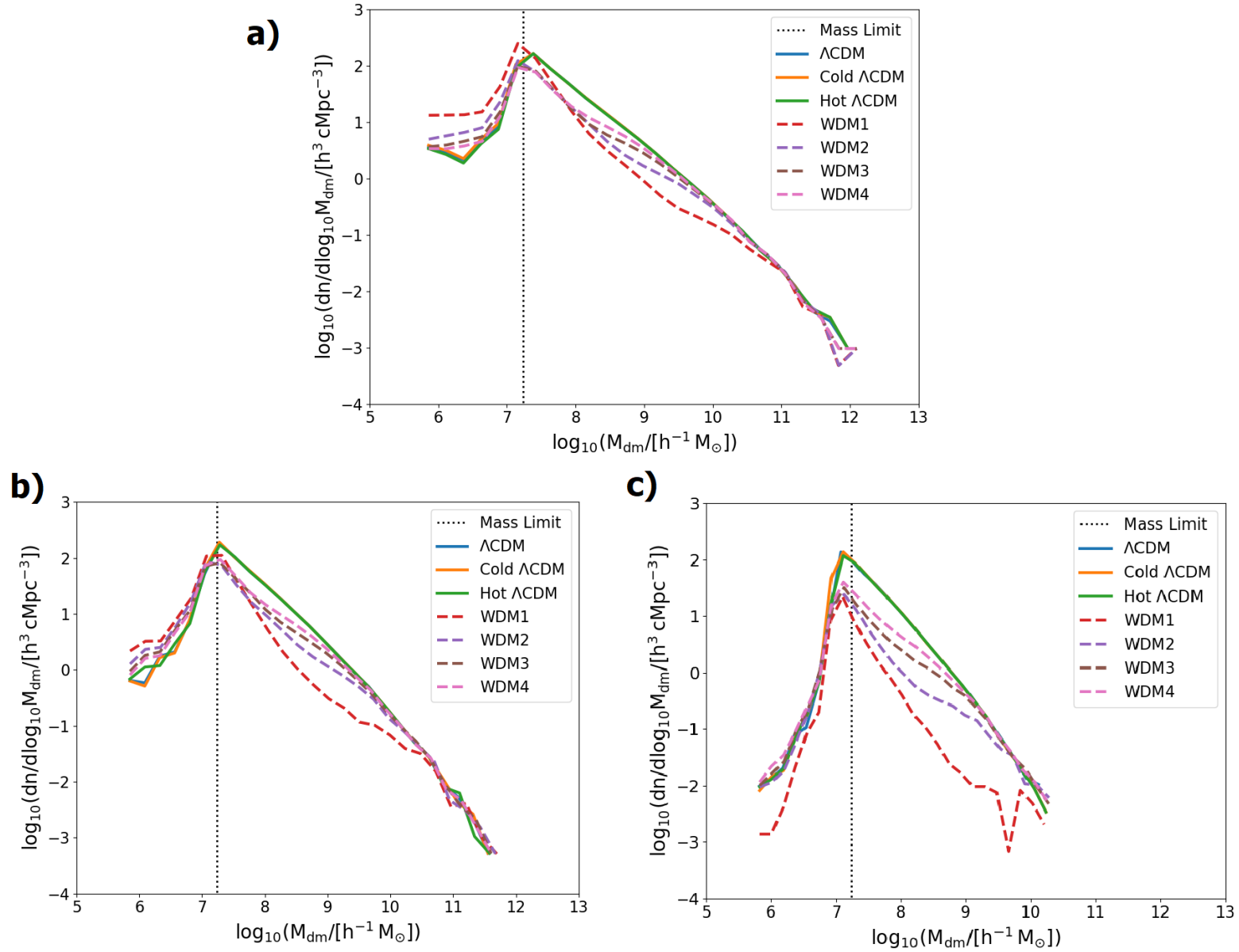
Figure 8 a, b, and c – Three plots showing the log density of halo masses for all dark matter models at redshifts of 4.2, 6, and 10 respectively. This is to illustrate how the size distribution of masses varies with z in different models.
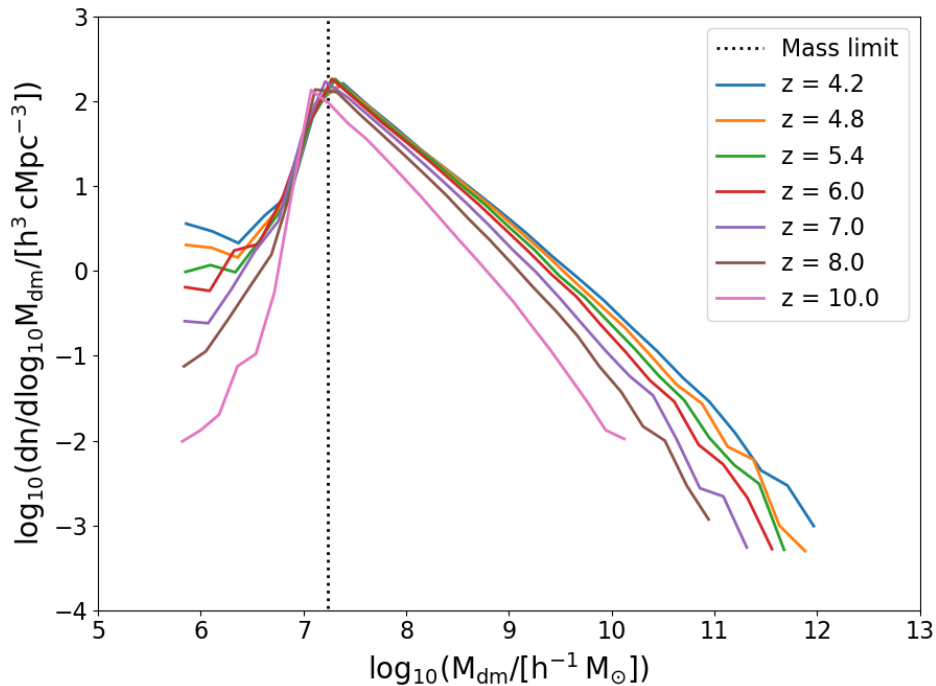

Figure 9 –A plot of the log density of log halo masses at all seven discrete values of redshift for which Sherwood-Relic halo mass data was available. These values are for the default ΛCDM model, but a similar pattern was seen for all models.

5.2 The ionizing efficiency parameter ζ

As shown in Equation 14, the value of emissivity (as its being calculated here) depends on the sum halo mass of the simulation volume and ζ, the ionizing efficiency parameter. This constant isn't a "real" physical quantity, but rather a free parameter tailored to the simulation being used. As such, it is calculated so as to give a "correct" value of emissivity at a specific redshift. It is expected that, at redshift 6, $\dot{n}_{ion} \approx 3 \times 10^{50}$ s^{-1} c Mpc^{-3} [27], and, as such, the value of the free parameter ζ being used in Equation 14 was calculated so as to ensure that an appropriate value of $\dot{n}_{ion}$ was found at z = 6. The values of ζ required to ensure that value of $\dot{n}_{ion}$ was being calculated is shown in Figure 10. The value of ζ taken from this plot was $1.031 \times 10^{41} s^{-1} M_\odot{}^{-1}$. This ζ value was later empirically calibrated to better align the ionization history shown in later figures with observed measurements of the ionization history [31]. This is necessitated by the relative simplicity of our model and the very nature of *simulating* a universe rather than measuring our own; in order to facilitate comparing the results found here against measured values from the literature [31], the ionizing efficiency parameter ζ must be adjusted as it is impossible to get a simulated universe to align perfectly with reality, especially when a major property (in this case, the fundamental properties of dark matter) is being varied.
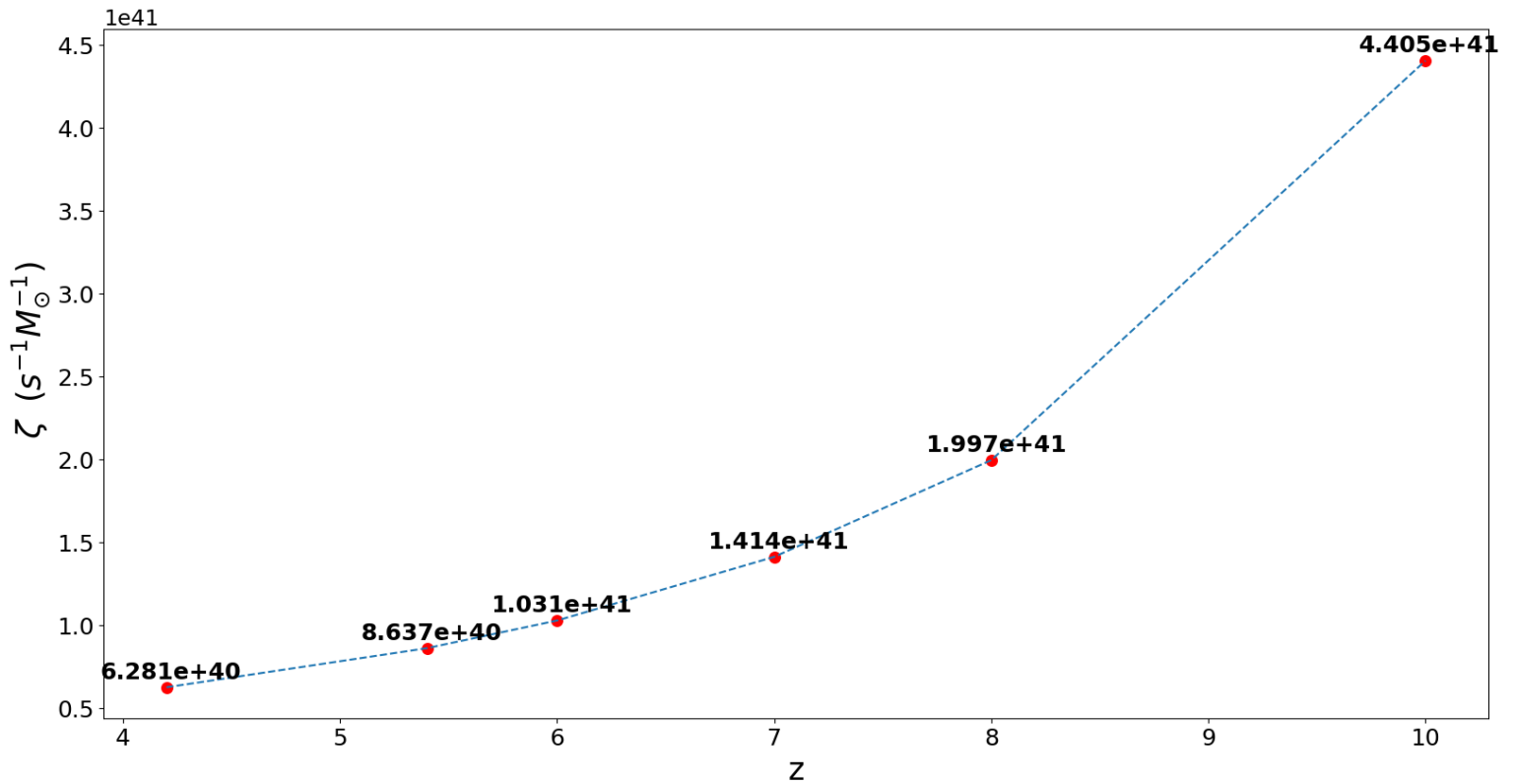

Figure 10 –A plot showing the values of the ionizing efficiency parameter required to find appropriate values of emissivity against redshift.

It was also demonstrated that the value of ζ required to guarantee an appropriate $\dot{n}_{ion}$ value had a dependence on the halo mass limit being used, as shown in Figure 11.
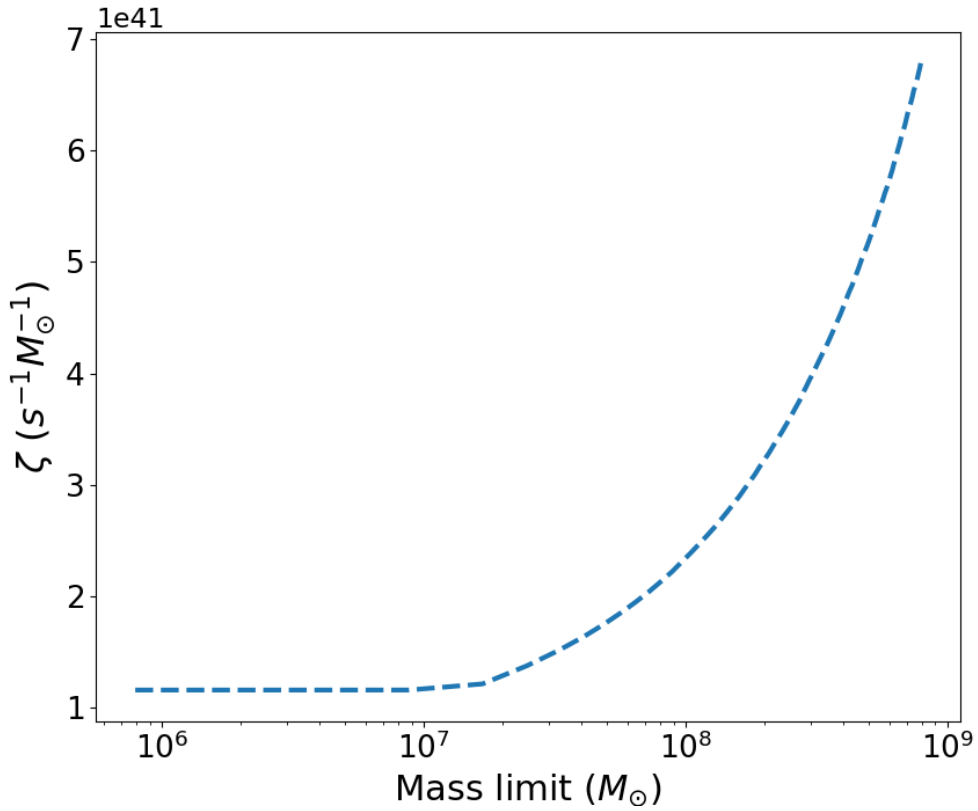
Figure 11 – A plot showing how the value of ζ varies with the mass limit. This plot is for a redshift of 6.

Using the same halo mass data used to produce Figures 10 and 11 and the ζ value found above, a set of $\dot{n}_{ion}$ values varying with redshift were calculated for each DM model via Equation 14 and are shown in Figure 12. As the files which were made available from the original simulations only measure the halo masses at certain discrete values of redshift (4.2, 4.8, 5.4, 6.0, 7.0, 8.0, and 10.0), specific points of gradient change can be seen and the $\dot{n}_{ion}$ values shown here (and from here on in, as these values are used in all following calculations where $\dot{n}_{ion}$ is needed) are not continuous.
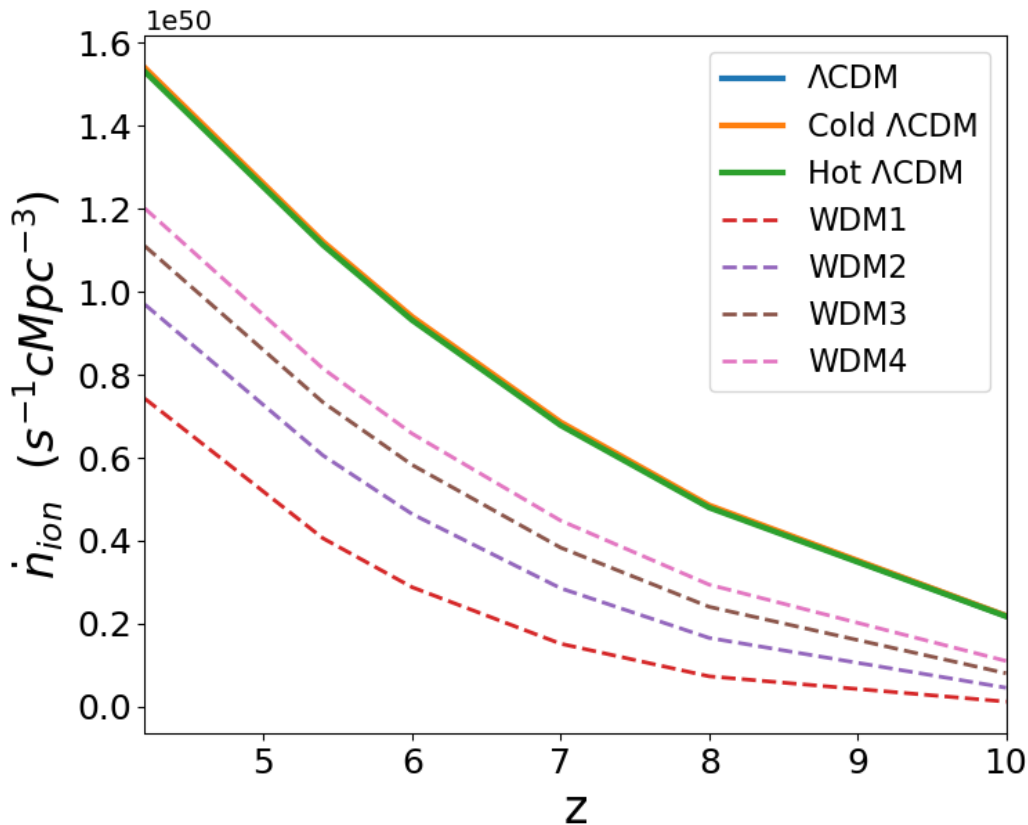

Figure 12 – A plot of the emissivity as calculated from the halo mass data of the Sherwood-Relics simulations as it varies with redshift, calculated in accordance with the value of ζ found in section 5.2.
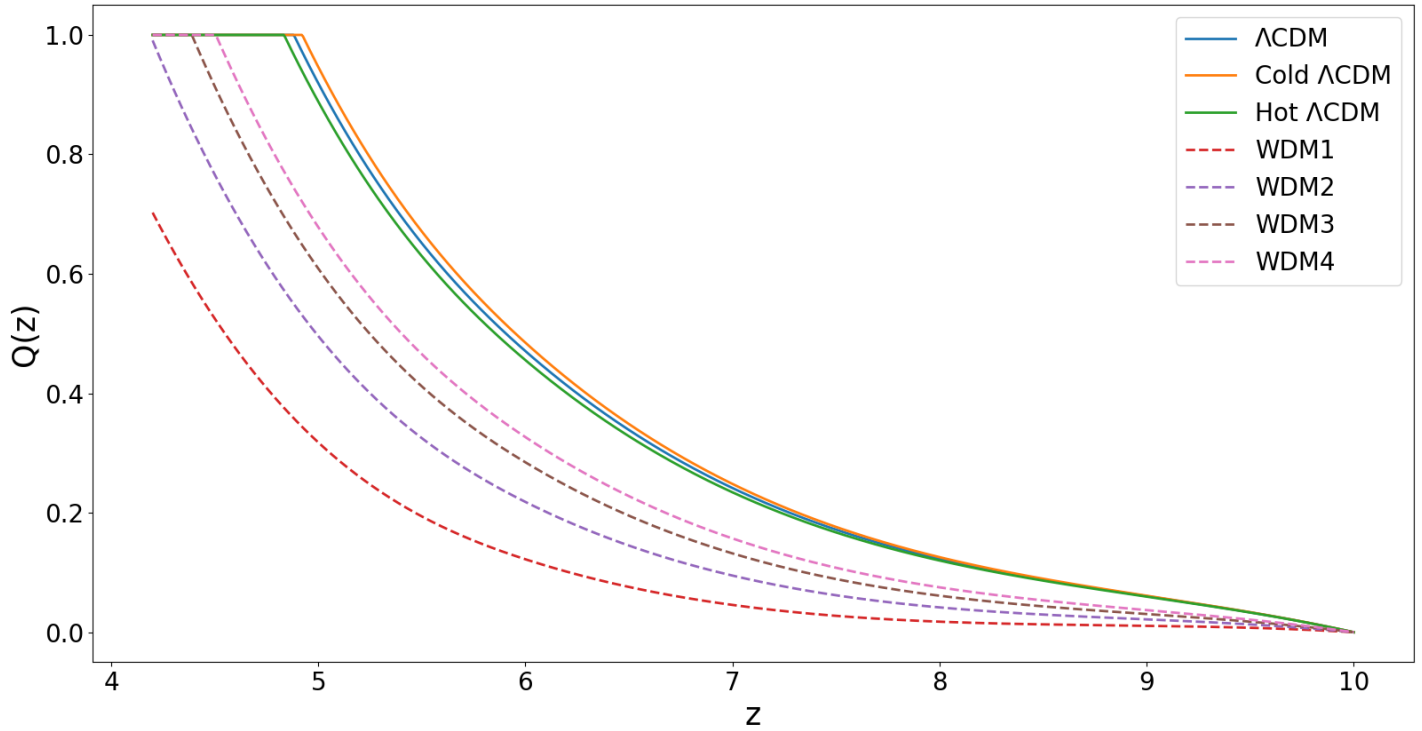
5.3 The uncalibrated ionization fraction

Figure 13 – A plot of the ionization fraction against redshift for all seven dark matter models.

The ionization fraction was first calculated with use of the values of C_R and $\dot{n}_{ion}$ for each dark matter model calculated above, and plotted against redshift, as shown in Figure 13. At any points where the value of Q exceeds 1, it was set to 1 automatically and understood to be a quirk of the mathematical modelling in the code. To do otherwise and allow the ionization fraction to exceed 1 would be completely unphysical, since it is the proportion of hydrogen within the volume which is ionized and it can't possibly be that that is over 100%.

5.4 The effect of the mass limit and exponent in Equation 14

Equation 14 [27] shows that $\dot{n}_{ion}$ is calculated with three adjustable parameters: the ionizing efficiency parameter ζ, the exponent α, and the mass limit, as described in Section 2.4. While it is generally agreed that ζ is the dominating factor in the calculation of $\dot{n}_{ion}$, it was thought worth investigating the extent to which the other two parameters effect the data being studied here, and as such ionization histories using several versions of each parameter were produced.
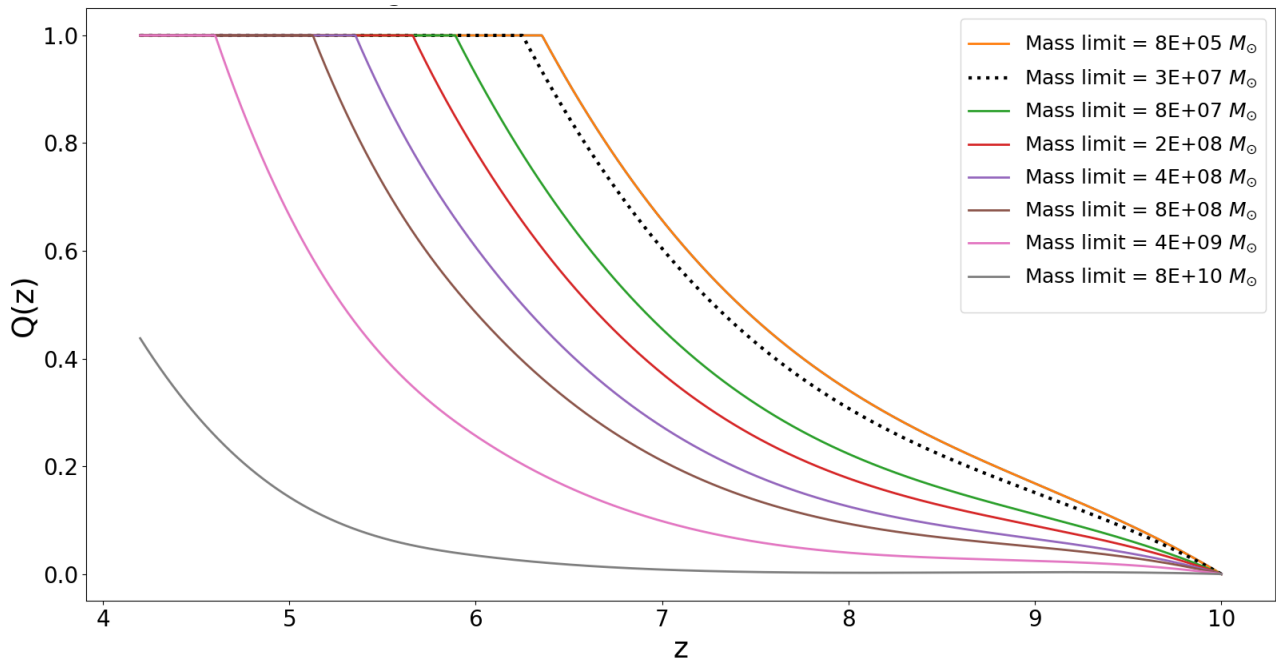
Figure 14 – A plot to illustrate the relationship between the ionization fraction and redshift and how that varies with the mass limit in use. The dotted line marks the resolution limit of the simulation. This was performed using the default ΛCDM model.
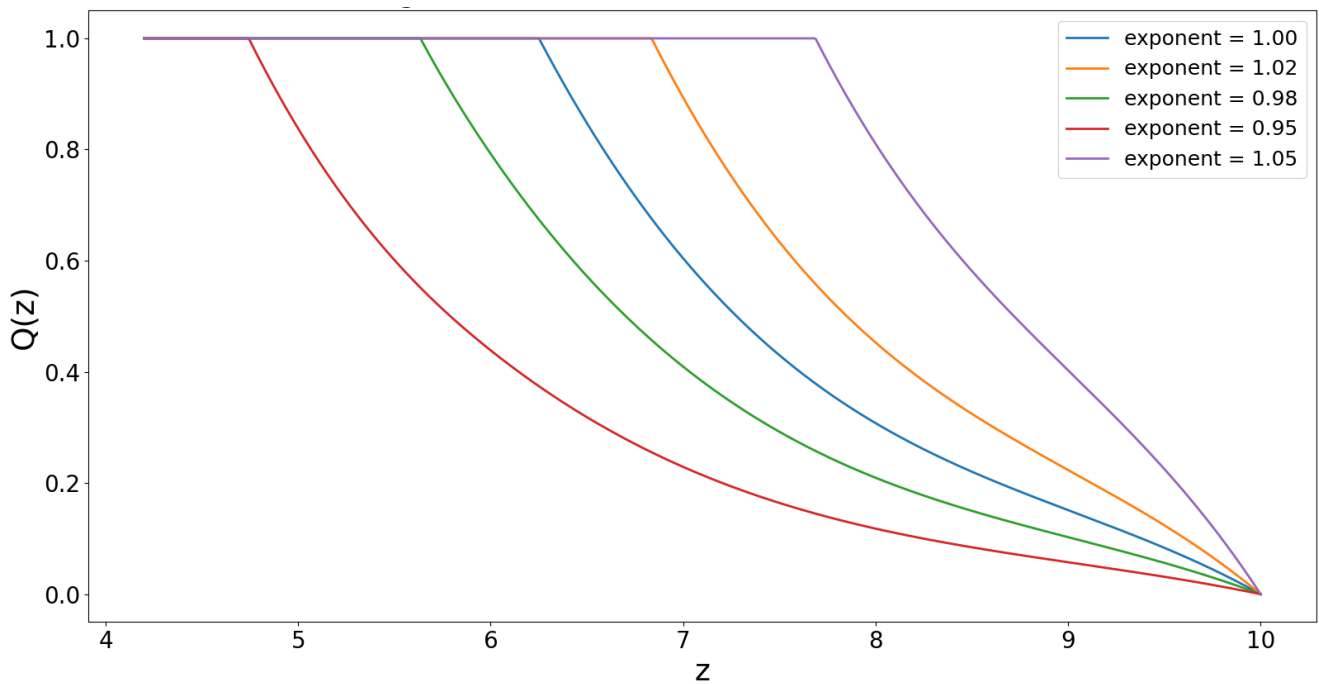

Figure 15 – A plot to illustrate the relationship between the ionization fraction and redshift and how that varies with a possible exponent on the sum halo mass in equation 14. This was performed using the default ΛCDM model.

As shown in Figure 14, raising the mass limit has the effect of deepening the curve and postponing the end of reionization while, as shown in Figure 15, lowering the exponent achieves the same effect, while raising it achieves the opposite. These two parameters are degenerate with one another, and their effect on the timing of the end of reionization can be sufficiently emulated by simply adjusting ζ. Ultimately, when compared to expected ionization curves [3,7], it was found that the these factors were not nessecary for the purposes of this investigation, and thus the exponent α was set to 1 and left unaltered, and the mass limit remained at the resolution of the simulation.

5.5 The ionization fractions compared to measured data

The ionization fraction was calculated again, this time using both the calculated, redshift-dependent values of the recombination clumping factor for each dark matter model, as calculated in Section 3.3, and an individual and mass-dependent set of values of $\dot{n}_{ion}$ for each model, as found in Section 5.2. These fully customised reionization histories are shown in Figure 16. Measured values of the ionization fraction were found by Šoltinský et al. [30] and added to the plot for comparison to real values and to determine whether it was appropriate to adjust the value of the free parameter ζ to move the reionization history slightly towards higher redshifts by verifying if the simulated ionization curves aligned well with measured values. Many of these HII fractions were in fact HI fraction measurements originally, but since there are only two possible states of hydrogen it is always true that $Q_{HI} + Q_{HII} = 1$, so HI fractions can easily be converted to HII fractions.
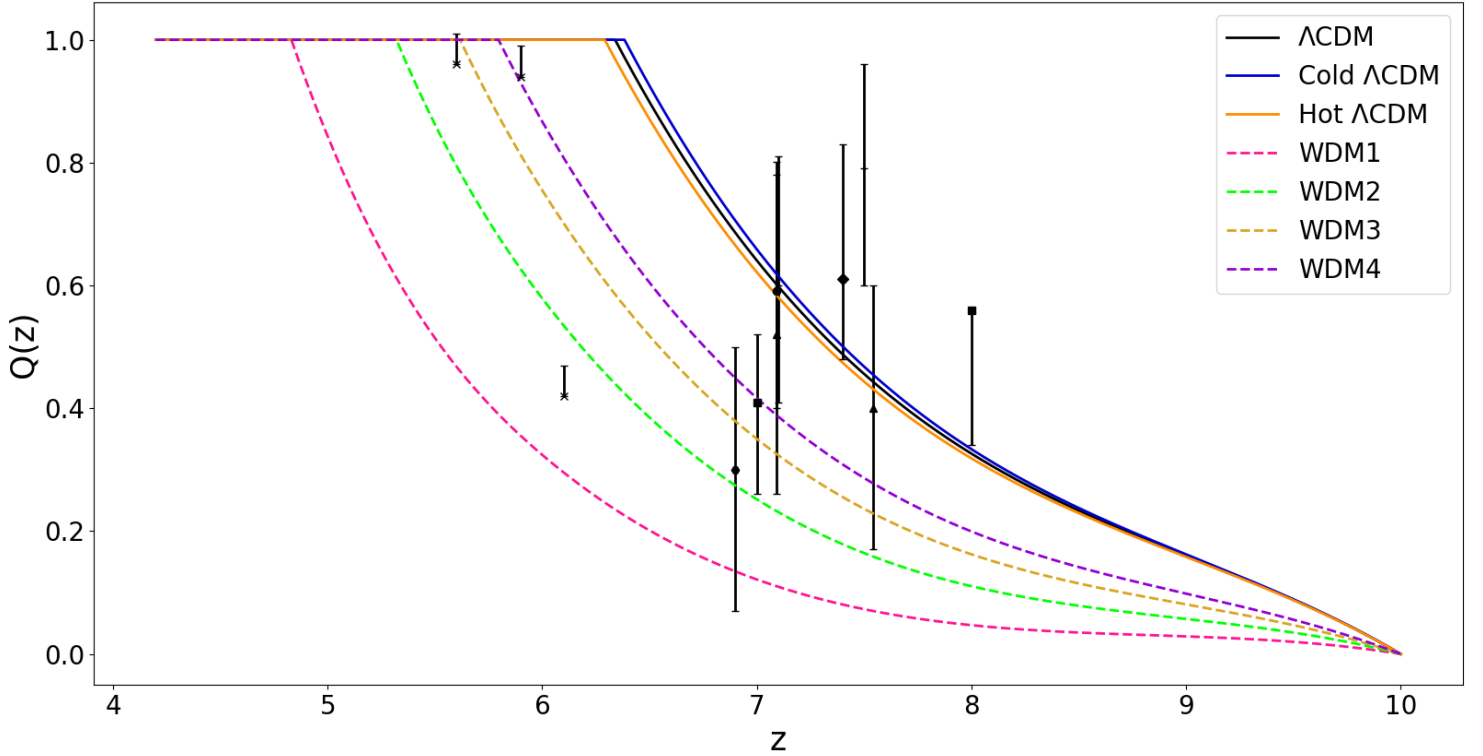

Figure 16 – A plot of the ionization fraction against redshift for all seven dark matter models as compared to (and calibrated in reference to) real HII fraction measurements. This data was gathered by Šoltinský et al [30]. The circular marker represents Bañados et al. (2018), the crosses represent McGreer et al. (2015), the diamond represent Yang et al. (2020), the hexagon represent Wang et al. (2020), the upwards triangles represent Davies et al. 2018, the pluses represent Greig et al. (2019), and the squares represent Mason et al. (2018, 2019). This information is not on the plot itself so as to avoid obscuring the data.

In light of the positions of the data displayed in Figure 16, and since ΛCDM is generally considered to be the standard [11], ζ was calibrated to $\zeta = 3.331 \times 10^{41} s^{-1} M_{\odot}^{-1}$ in order to align the real HII fraction measurements with the ionization histories of the ΛCDM models.

5.6 The impact of C on the ionization fraction

The value of Q was then calculated using the exact same set of C values (those calculated the default ΛCDM) for each dark matter model, but while still using correctly calculated values of $\dot{n}_{ion}$ and the value of ζ used in Figure 16. This was done to compare the impact of the clumping factor on the ionization history as compared to that of the emissivity and is shown in figure 17.
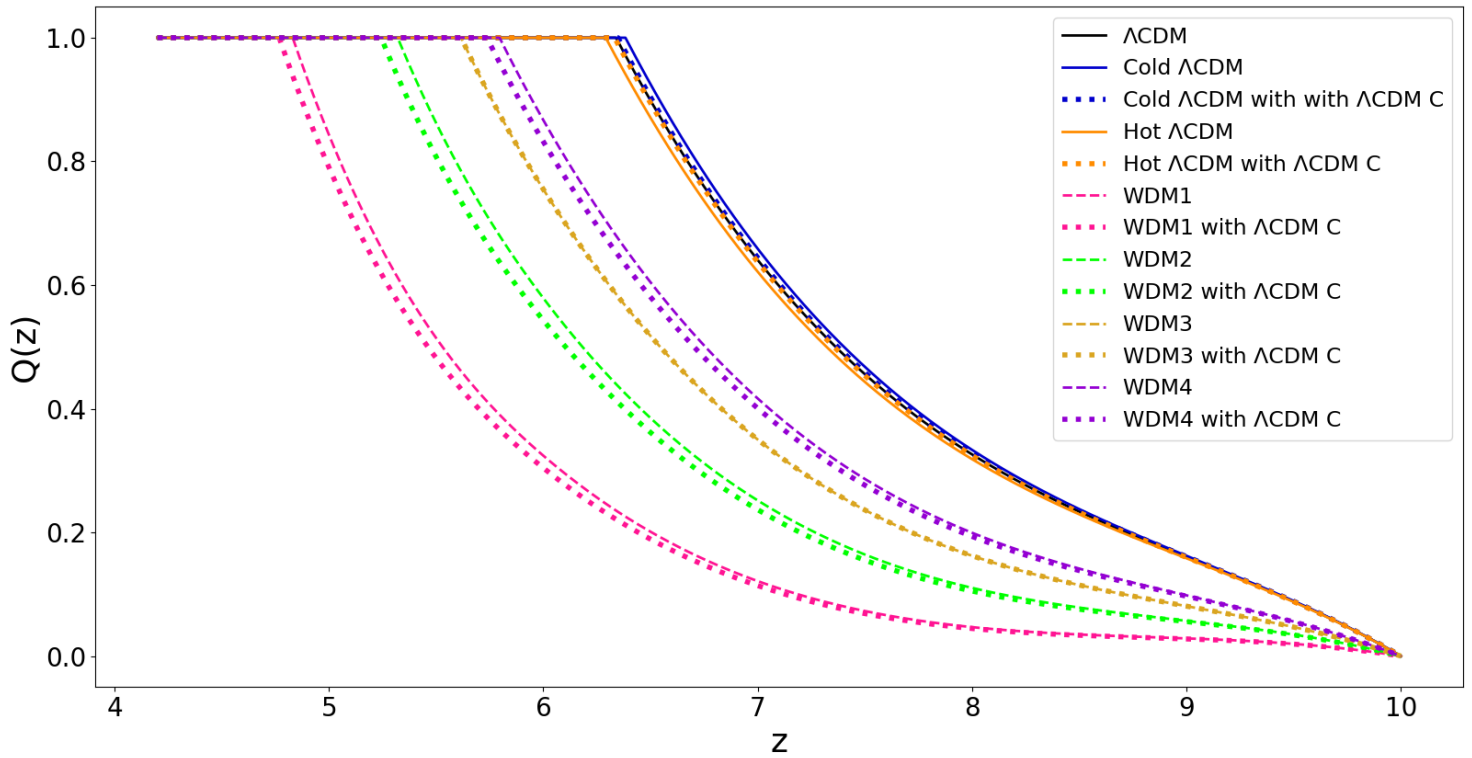
Figure 17 – A plot showing the ionization fraction against redshift for all seven dark matter models in comparison to those same ionization fractions instead calculated with identical clumping factors for each of them.

5.7 Discussion

The mass bin plots in Figure 8 and 9 show the effects on halo masses and structure which would be expected from the theory. Figure 9 shows far less large-scale structure at a high redshift, which agrees with theory in that structure is hierarchical. Large-scale structure is built upon small-scale structure; small collections of halo masses grow into larger ones over time under the effect of gravity. This is reassuring in that to see otherwise would outright defy physical principles and imply some relatively extreme problems in the simulation of the halo masses or in our handling of that data. The plots in Figure 8 show each model in direct comparison at the same redshifts, and in each, all the WDM models show a lesser number of low mass halos, with the $1keV/c^2$ WDM model always having the least and $4keV/c^2$ always having the most (out of the WDM models). This aligns well with the theory outlined in Section 2.1 which predicts that a lower mass candidate should translate to more pronounced small-scale structure suppression, coming from how the original density field perturbations and mass power spectrums change with mass - the higher pass particles require less force to settle into structure and so form low mass structures as well as high, whereas the low mass particles have a higher velocity due to their free streaming scale and require a more intense gravitational pull to settle into structure, and so they mostly cluster together into larger-scale structure [10, 11]. This trend is present in each plot but is less clear in Figure 8c where z = 10, because large-scale structure has not yet had as much time to form in any of the models. It can be safely said that, although the WDM curve is somewhat more unpredictable than the others throughout due to having the highest free streaming scale, the spike at approximately $log_{10}M_{dm}$ = 9.5 can be taken as an anomaly of the simulation arising from its perturbation generation rather than a reflection of real WDM halo mass behaviour. Anything before the dotted line of approximately $2.53 \times 10^7 \, M_\odot$ is below the mass resolution of the simulation, and so, although that

portion of the plot can give an intresting impress of what might be happening, it cannot be considered fully reliable and is projection beyond that limit.

Figure 9 shows that the ionizing efficiency parameter, ζ, is dependent on redshift, which aligns with theory – from Equation 14 it can be seen that, when $\dot{n}_{ion}$ is held constant, ζ would be expected to vary with z to compensate for the fact that $\sum_i (M^i)$ does. The value of ζ here was only calibrated in respect to the emissivity expected at redshift 6, meaning that it is certainly inaccurate at earlier times and could be improved upon through use of dynamic adjustment. Figure 11 also shows that ζ depends upon the mass limit in use, and so, as the original $\dot{n}_{ion}$ value is appropriate for a system which takes $9.41 \times 10^7 \ M_\odot$ as the limit [8], this should have been taken into consideration while calibrating ζ – it was not, which likely led to inaccuracies. Even within this simplified model of emissivity and its reliance on halo mass, this is an area which was somewhat mishandled and could quite easily see major improvement by taking mass limit and redshift variance into account in the value of ζ. However, the largest source of error is the simple emissivity model [27] itself – there are many other methods of normalizing the mass-emissivity relationship [7, 11] and by not taking them into individual consideration the ionization histories found here cannot be realistically complete.

Figure 12 displays a pattern in the DM models' emissivity wherein the curves are of practically identical shapes but are arranged in order of particle mass, with the lightest, WDM1, having the lowest emissivity at all points and the CMD models, being much heavier, having the highest. As shown in Equation 14, $\dot{n}_{ion}$ is deeply dependant on the sum of the total halo masses within the simulation volume, so this aligns well with the theory. Predictably, as the only thing differentiating the CDM models is their temperature, their $\dot{n}_{ion}$ curves are identical – there are some very minimal places in which the three CDM curves don't completely overlap, but these are minute enough to be quite easily dismissed as a graphing error rather than anything physical. All $\dot{n}_{ion}$ values found are of the correct magnitude when compared to other research [8], which can be taken as further assurance that the cosmological understanding being used to obtain these values is sound and that the ζ value in use is valid.

Figure 13, the first time that the reionization history is plotted with full sets of data for this simulation, shows good signs in regards to the data and its handling; the general shape of the curves are appropriate as seen in Figure 9 and the literature [3, 7], and although the reionization timing *is* too early, this was expected and easily fixed by further calibrating the free parameter ζ. The duration of reionziation is also much more realistic here than it was prior in Figure 9.

The act of changing the mass limit during the calculation of Q, as in Figure 14, is questionable given that, as shown in Figure 11, the ionizing efficiency parameter ζ is also dependant on the mass limit in use and while the mass limit being used to calculate Q was being altered, the constant value of ζ found in Section 5.2 at a mass limit of $2.53 \times 10^7 \ M_\odot$ was still in use since this process was spread over several files and computers and altering ζ in accordance to mass limit would have been a great difficulty. As such, these measurements show the likely change in trend which varying the mass limit would cause, but can't be assumed to be completely accurate. When combined with Figure 15, this demonstrates that this method of calculating Q is by far dominated by the $\dot{n}_{ion}$ component and that changing factors in other parts of the ionization equation (Equations 1 and 2) is unlikely to have a comparatively signifigant effect. The fact that the parameters aside from ζ which were investigated were found to be degenerate and largely irrelevant aligns well with prior research [27, 20].

The reionization histories presented in Figure 16 line up relatively well with the measured HII fraction data – every curve is within the error bars of at least one point and all of the CDM curves (and some of the WDM curves) are within two standard deviations of a majority of the data points, so these results are certainly of the correct magnitudes and, while extremely unlikely to be numerically correct due to coming from simulation data, are quite accurate to the trends seen in reality. It is also worth noting how widely dispersed the measured data points are and the size of their error bars; this is a quantity which is difficult to measure and on the cutting edge of a contentious field, making *any* research building on this area relatively valuable.

Since the free parameter ζ was calibrated in reference to the CDM models, the WDM models are further from the data points. This does not necessarily imply what CDM is more likely to be accurate in reality, but the measured data as compared to our curve do show that, in order for WDM to be a viable model of dark matter, a much higher ionising emissivity would be required as compared to that in a CDM universe, meaning either a much higher sum halo mass or photoionization efficiency per unit mass would be necessary, indicating that those are two strong quantities which could be monitored to discern which dark matter models are more likely to be in effect in the real universe.

The numeric redshift value at which ionization finishes in these figures cannot be directly compared as that had been empirically adjusted between the almost proof-of-concept plot in Figure 9 and the more realistic Figure 13. What *is* relevant and comparable is the shape, gradient, order, and relative proximity of the curves. The order of the curves has been reversed. Previously, when $\dot{n}_{ion}$ was taken as a constant value, the CDM models finished ionization last, in the order of cold to hot, and the WDM models finished earlier, with the lightest, WDM1 leading the pack. All of those curves were very close together, especially the WDM ones. Here the lightest WDM models complete ionization *last* while the CDM models finish significantly earlier (although, it is worth noting that the arrangement has not completely flipped; the three CMD ionization histories are still in the same order and still very close together). Also, the WDM models' histories are much further from one another and from those of the CDM models. Effectively, what has changed between Figures 9 and 13 is that the former only took account of varying C values, whereas the latter uses individually tailored $\dot{n}_{ion}$ arrays. The fact that emissivity is such a strong factor in reionization that its inclusion can completely rearrange the reionization curves and change the duration of reionization (as seen in the shape and gradient of the curves – those in the $\dot{n}_{ion}$ adjusted plot are far steeper, showing that reionization takes place over a shorter period) heavily implies that $\dot{n}_{ion}$ is a vital and likely dominating factor in determining the characteristics of ionization history.

This is reinforced by the fact that the three CDM models are identical aside from their average temperatures, and as such, due to having the exact same mass, their $\dot{n}_{ion}$ values are also identical. Temperature only effects the clumping factor, and as such the only difference between the hot, cold, and default CDM models' reionization histories is the effect of C, hence them being so similar further suggests that clumping factor is relatively insignificant in these investigations. Altogether, this quite solidly indicates the answer to some of this investigation's basic questions: yes, dark matter models do affect the progress of ionization significantly, and yes, observation of the ionization fraction likely could be used to discern dark matter models.

Figure 17 shows the most conclusive evidence found in this investigation: the fact that a DM model's reionization history, when calculated with a set of incorrect values of C, is almost identical (and in one case *is* identical) to one calculated with the correct values of C. This is an extremely clear sign that the emissivity is by far the dominating factor in the reionization history and that the clumping factor is inconsequential in comparison. It was a valid assumption of prior research to ignore the variation of C with redshift [20].

Although, since they are not perfectly identical, this plot does suggest that the clumping factor could potentially be relevant during the investigation of the reionization history of multiple dark matter models which are identical in mass (like our CDM models, which, when the difference in C is removed, lay precisely on top on one another as expected) in which case the clumping factor would be the only way to differentiate them, or when investigating any DM model over a very small range of redshifts, where the small difference that the clumping factor makes could be significant in comparison to that small scale.

6   Overall discussion and uncertainty

6.1 Uncertainty

This being a theoretical investigation, there are no numeric uncertainties to be evaluated here (aside from the error bars on the data in Figure 16, but those were provided by the papers referenced and have little relevance to this investigation). However, uncertainties do arise from any inaccuracies or shortcuts in the method we have used. The most obvious of these is the approach taken to assessing photoionizing emissivity – Equation 14 is an extremely simple model of a complex relationship and it is highly likely that this is where the majority of the uncertainties in this project originate.

Emissivity is vital. Every step of this investigation has pointed to emissivity being the dominating factor in the progress of ionization. It is not a factor to make mistakes or assumptions about if it can be avoided. This is confirmed by this investigation itself, which has found $\dot{n}_{ion}$ to dominate reionization by a large margin.

While Equation 14 only has two parameters which can be used to refine the relationship between emissivity and mass, both of which need to be calibrated with regard to the data in use, the model developed by Hassan et at. [29] for example, has four, each with well-defined values rigorously determined by through use of a Schechter function and then minimising for ideal fits. This allows a much higher amount of flexibility and is more likely to represent emissivity correctly due to the sophisticated way in which it incorporates a superlinear ionization rate. As the exponent α was ultimately set to 1 here, for the sake of this investigation it has essentially been taken that $\dot{n}_{ion} \propto \sum M_H$ with a constant of proportionality ζ, which is a drastically incompletely way to model such an vital and relatively unknown relationship which, as seen in Section 5, practically dictates reionization.

The ionizing efficiency parameter ζ used in Equation 14 and throughout Section 5 accounts for the effect of many factors, which cannot possibly be modelled well by a single valued variable. The things contained within that one quantity (the star formation fraction, the emissivity escape fraction, the baryon fraction, and almost certainly others [7, 11] - anything that influences the relationship between halo mass and the production rate of ionizing photons is dictated by ζ in this model) are too many, and each too complex, to be correctly represented within one variable.

Another source of uncertainty surely comes from ζ being taken as a constant value of $3.331 \times 10^{41} s^{-1} M_\odot{}^{-1}$. It was shown in Figure 10 that ζ varies with redshift, which is confirmed in the literature [11] – in fact it varies strongly with redshift, both in our simple model and in more complex ones like Hassan et al.'s [29], and a complete understanding of ionizing efficiency cannot be found without modelling that relationship. This, of course, also impacts $\dot{n}_{ion}$, as ζ is a major factor in the emissivity value.

6.2 Opportunities for future research

When considering future research, the most obvious and likely most impactful way to improve our investigation would be to implement a more sophisticated fit with which to calculate emissivity – swapping the simple model used here (Equation 14) with a more complex model like, for example, the star formation rate model by Robertson et al. [31] or the prior discussed Hassan fit. [29]. Since this is such a burgeoning and often ill-defined field, it may even be worthwhile to investigate and define that relationship independently to compare against established research.

Additionally, it would be pertinent investigate the role played by the Thomson electron scattering depth, τ_e, which, being a quantity easily measured in the modern day, could serve as a very helpful barometer to assess whether the results being found from the simulations are similar to reality, as in [7, 15]. A real, measured value against which to compare these results would be very reassuring and provide a starting point for making any changes to the way the data is being processed, a test case to monitor if those changes had improved or diminished accuracy, and potentially as another quantity by which to compare DM models. τ_e would also be a particularly helpful value to compute since the real measurement is extremely precise as far as cosmological measurements go, at τ_e = 0.054 ± 0.007 [32] - there is far less room for error in τ_e than the massive error bars on the measured data shown in Figure 16. It is also a fairly useful value in to have more information on itself as it can be used to determine the amplitude of the mass power spectrum fluctuations [16], which is in turn helpful for exploring WDM and small-scale structure suppression (as mentioned in section 2.1).

This is a little-explored area which has only recently become viable to explore in this capacity at all, and which we gain more ability to understand every year that cosmological simulation technology becomes more advanced and more available. Given the grand scales on which cosmology as a field operates, many quantities and phenomena of interest are currently immeasurable practically, and when they're not, the measurements are usually far from certain or precise, as can be seen from both the spread of the data and the size of the error bars in Figure 16. An aim in this investigation was to verify that the theory currently in use matches up with what is seen in practice and that the equations used are an approximately correct way to process the data obtained from simulations like those of the Sherwood-Relics Project. Both ideas were confirmed. It was also hoped that this data could help illuminate the relationships between various dark matter models and ionization, and to investigate ways to differentiate them (which can be addressed relatively soundly through trends and contrast alone), which was accomplished. All of this is based largely on cutting edge research from the last few years [1, 3, 7, 23]. Also, in the process of this investigation one factor in the modelling and study of dark matter and reionization, the clumping factor, was practically eliminated as a significant concern and others were highlighted as much more likely to be of consequence, those being the total halo mass and the photoionization efficiency per unit mass.

In regards to how this investigation has answered the initial questions of this investigation: the clumping factor absolutely varies with dark matter model, the specifics of which is demonstrated in Figure 5 and Section 3, and is best modelled specifically to recombination, as in Equation 6. The clumping factor also slightly impacts the universe's ionization history, as shown in Figure 17, but is almost completely overwhelmed by the photoionizing emissivity $\dot{n}_{ion}$, which is the dominating factor in the ionization fraction by a long margin.

Ionization histories are influenced significantly by the dark matter model in use, with more stark differences occurring between WDM models due to their differing particle masses and free streaming scales being a direct factor in $\dot{n}_{ion}$, and the degree to which DM models impact ionization history is very likely significant enough to allow dark matter models to be distinguished through observation of the HII fraction.

It is almost impossible for these to be numerically precise answers, due to this being both a theoretical investigation and one based on simulations, but it can be safely said that the trends found here are approximately representative of reality and that this and similar investigations can be used as a suitable (although it could certainly be improved) way to determine which factors in reionization are of particular significance, and to evaluate which avenues of cosmological research may be more worth pursuing.

7 Conclusion

The Sherwood-Relic Project's suite of hydrodynamical cosmological IGM simulations were used to examine the cosmic reionization of hydrogen and how that reionization is affected by different models of dark matter. This was investigated at a density limit of 100 and a mass limit of $2.53 \times 10^7 \, M_\odot$ by using several of the most likely dark matter models [3]. The limits of this investigation were the use of a relatively very simple model of ionizing emissivity [27] as compared to, for instance, Robertson or Hassan [31, 29]. Also, a constant rate of ionising emissivity per unit halo mass was used, which is absolutely unphysical and should exhibit a wide variance.

The main focus of this project was to question the current convention of the field, which dictates that ignoring the fluctuations of the clumping factor with redshift when investigating reionization histories, under the assumption that emissivity is the dominating factor in the progress of reionization. As shown in Figure 17, this is a valid assumption, as, while C does affect the ionization fraction and the duration of reionization, the changes it causes are very slight, while the effects of emissivity overwhelm it. While there are points (between approximately redshift 5 and 7) where C has a slightly larger impact, it is still a valid approach to ignore the clumping factor when simulating dark matter in respect to reionization over a large timescale, especially when using warm dark matter models.

It was also found that different dark matter models absolutely impact the progress of reionization, completely changing its timing and duration, although it does always follow a similar trend. It was shown that the lighter the particle being used, the later reionization will finish and the longer it will take finish. This difference is quite marked between models which have different particle masses but is also present between an identical model at different temperatures, due to the relationship between temperature, pressure, and homogeneity in the IGM.

Due to this, it is possible to distinguish between dark matter models via observation of the reionization fraction as it changes with redshift, particularly between WDM models which exhibit more signifigant variance. These results largely agree with current research [7, 27]. This indicates that the theory and methods laid out here are broadly sound, that the Sherwood-Relics project's simulations are reliable and accurate, and that the data it can provide has are insightful, accurate to other simulations in the field, and in strong agreement with the trends see in the real, measured universe, but this investigation could be elaborated upon by investigating the Thomson electron scattering depth, as seen in similar literature [29, 15, 7], using a more realistic, non-constant relationship of emissivity and mass or more fully considering the other factors with comprise our parameter ζ (as discussed in Section 6.1), and by calculating photoionizing emissivity in reference to other factors [31, 20] or with deeper complexity[29].

References

[1] N. Y. Gnedin and P. Madau, "Modeling cosmic reionization," *Living Reviews in Computational Astrophysics*, vol. 8, no. 1, Nov. 2022.

[2] X. Fan, M. A. Strauss, R. H. Becker, R. L. White, J. E. Gunn, G. R. Knapp, G. T. Richards, D. P. Schneider, J. Brinkmann, and M. Fukugita, "Constraining the evolution of the ionizing background and the epoch of reionization with $z \sim 6$ quasars. II. A sample of 19 quasars," *The Astronomical Journal*, vol. 132, no. 1, pp. 117–136, Jul. 2006.

[3] E. Puchwein, J. S. Bolton, L. C. Keating, et al., "The Sherwood-relics simulations: Overview and impact of patchy reionization and pressure smoothing on the intergalactic medium," *Monthly Notices of the Royal Astronomical Society*, pp. 1–23, Dec. 2022.

[4] "Sherwood-Relics," *The Sherwood-Relics Project*. [Online]. Available: https://www.nottingham.ac.uk/astronomy/sherwood-relics/. [Accessed: 23-Jan-2023].

[5] J. S. Bolton, E. Puchwein, D. Sijacki, M. G. Haehnelt, T.-S. Kim, A. Meiksin, J. A. Regan, and M. Viel, "The Sherwood Simulation Suite: Overview and data comparisons with the Lyman α forest at redshifts 2 ≤z≤ 5," *Monthly Notices of the Royal Astronomical Society*, vol. 464, no. 1, pp. 897–914, Sep. 2016.

[6] "About," *The Sherwood-Relics Project*. [Online]. Available: https://www.nottingham.ac.uk/astronomy/sherwood-relics/about.php. [Accessed: 23-Jan-2023].

[7] N. Chen, A. Doussot, H. Trac, and R. Cen, "Scorch. III. analytical models of reionization with varying clumping factors," *The Astrophysical Journal*, vol. 905, no. 2, pp. 132–146, Apr. 2020.

[8] L. C. Keating, E. Puchwein, and M. G. Haehnelt, "Spatial fluctuations of the intergalactic temperature–density relation after hydrogen reionization," *Monthly Notices of the Royal Astronomical Society*, vol. 477, no. 4, pp. 5501–5516, Jul. 2018.

[9] A. Jeeson-Daniel, B. Ciardi, and L. Graziani, "Clumping factors of H II, he II and HE III," *Monthly Notices of the Royal Astronomical Society*, vol. 443, no. 3, pp. 2722–2732, Jul. 2014.

[10] S. Paduroiu, Y. Revaz, and D. Pfenniger, "Structure formation in warm dark matter cosmologies: Top-Bottom Upside-Down." *arXiv preprint*, Jun. 2015

[11] P. Villanueva-Domingo, N. Y. Gnedin, and O. Mena, "Warm dark matter and cosmic reionization," *The Astrophysical Journal*, vol. 852, no. 2, pp. 139–146, Jan. 2018.

[12] J. S. Bullock and M. Boylan-Kolchin, "Small-scale challenges to the λCDM paradigm," *Annual Review of Astronomy and Astrophysics*, vol. 55, no. 1, pp. 343–387, Jul. 2017.

[13] K. Finlator, L. Keating, B. D. Oppenheimer, R. Davé, and E. Zackrisson, "Reionization in technicolor," *Monthly Notices of the Royal Astronomical Society*, vol. 480, no. 2, pp. 2628–2649, 2018. doi:10.1093/mnras/sty1949

[14] M. Klasen, M. Pohl, and G. Sigl, "Indirect and direct search for dark matter," *Progress in Particle and Nuclear Physics*, vol. 85, pp. 1–32, 2015. doi:10.1016/j.ppnp.2015.07.001

[15] E. Puchwein, F. Haardt, M. G. Haehnelt, and P. Madau, "Consistent modelling of the meta-galactic UV background and the thermal/ionization history of the intergalactic medium," *Monthly Notices of the Royal Astronomical Society*, vol. 485, no. 1, pp. 47–68, 2019. doi:10.1093/mnras/stz222

[16] G. P. Holder, Z. Haiman, M. Kaplinghat, and L. Knox, "The reionization history at high redshifts. II. estimating the optical depth to Thomson scattering from cosmic microwave background polarization," *The Astrophysical Journal*, vol. 595, no. 1, pp. 13–18, 2003. doi:10.1086/377338

[17] "About," The Sherwood-Relics Project. [Online]. Available: https://www.nottingham.ac.uk/astronomy/sherwood-relics/about.php. [Accessed: 23-May-2023].

[18] A. Schneider, "Dark Matter Structures and the Free Streaming Scale", dissertation, Institute for Theoretical Physics, University of Zurich, 2012. [Online].
Available: https://www.zora.uzh.ch/id/eprint/75587/1/20131701.pdf [Accessed: 23-May-2023].

[19] H. N. Nguyễn, N Sehgal, M. S. Madhavacheril, "Measuring the small-scale matter power spectrum with high-resolution {CMB} lensing", *Physical Review D*, vol. 99, no. 1, 2019

[20] P. Madau, F. Haardt, and M. J. Rees, "Radiative transfer in a clumpy universe. III. the nature of cosmological ionizing sources," *The Astrophysical Journal*, vol. 514, no. 2, pp. 648–659, 1999. doi:10.1086/306975

[21] A. A. Kaurov and N. Y. Gnedin, "Cosmic reionization on computers. III. the clumping factor," *The Astrophysical Journal*, vol. 810, no. 2, p. 154, 2015. doi:10.1088/0004-637x/810/2/154

[22] A. Jeeson-Daniel, B. Ciardi, and L. Graziani, "Clumping factors of H II, he II and HE III," *Monthly Notices of the Royal Astronomical Society*, vol. 443, no. 3, pp. 2722–2732, Jul. 2014.

[23] J. H. Wise, "Cosmic reionisation," *Contemporary Physics*, vol. 60, no. 2, pp. 145–163, May 2019.

[24] A. A. Kaurov and N. Y. Gnedin, "Recombination clumping factor during cosmic reionization," *The Astrophysical Journal*, vol. 787, no. 2, pp. 146–152, Apr. 2014.

[25] A. H. Pawlik, J. Schaye, and E. van Scherpenzeel, "Keeping the universe ionized: Photoheating and the clumping factor of the high-redshift intergalactic medium*," Monthly Notices of the Royal Astronomical Society*, vol. 394, no. 4, pp. 1812–1824, Jan. 2009.

[26] D. A. Verner, G. J. Ferland, "Atomic data for astrophysics. I. Radiative recombination rates for H-like, He-like, Li-like, and Na-like ions over a broad range of temperature", *The Astrophysical Journal Supplement Series,* vol. 103. pp. 467-473, Apr. 1996.

[27] G. Kulkarni et al., "Large Lyman-α opacity fluctuations and low CMB τ in models of late reionization with large islands of neutral hydrogen extending to z < 5.5," *Monthly Notices of the Royal Astronomical Society: Letters,* vol. 485, no. 1, 2019. doi:10.1093/mnrasl/slz025

[28] K. Finlator, B. D. Oppenheimer, and R. Davé, "Smoothly rising star formation histories during the reionization epoch," *Monthly Notices of the Royal Astronomical Society*, 2010. doi:10.1111/j.1365-2966.2010.17554.x

[29] S. Hassan, R. Davé, K. Finlator, and M. G. Santos, "Simulating the 21cm signal from reionization including non-linear ionizations and inhomogeneous recombinations," *Monthly Notices of the Royal Astronomical Society*, vol. 457, no. 2, pp. 1550–1567, 2016. doi:10.1093/mnras/stv3001

[30] T. Šoltinskí et al., "The detectability of strong 21 centimetre forest absorbers from the diffuse intergalactic medium in late reionisation models," *Monthly Notices of the Royal Astronomical Society*, 2021. doi:10.1093/mnras/stab1830

[31] B. E. Robertson, R. S. Ellis, S. R. Furlanetto, and J. S. Dunlop, "Cosmic reionization and early star-forming galaxies: a joint analysis of new constraints from Planck and the Hubble Space Telescope", *The Astrophysical Journal*, vol. 802, no. 2, 2015. doi:10.1088/2041-8205/802/2/l19

[32] N. Aghanim et al., "Planck2018 results," *Astronomy & Astrophysics*, vol. 641, 2020. doi:10.1051/0004-6361/201833910